การจำลองการเคลื่อนที่แบบ 3 มิติ ของอนุภาคเดี่ยว ตามการไหลแบบปั่นป่วน
ในก๊าซไซโคลนแบบเป่าลง

นายกัมปนาท แก้วปลั่ง

SIMULATION OF SINGLE PARTICLE MOTION ALONG 3-DIMENSIONAL
TURBULENT FLOW IN AIR CYCLONE WITH BLOWDOWN

Mr. Kompanart Kaewplang

Thesis Title   SIMULATION OF SINGLE PARTICLE MOTION ALONG 3-DIMENSTIONAL TURBULENT FLOW IN AIR CYCLONE WITH BLOWDOWN

By   Mr. Kompanart Kaewplang

Field of Study   Chemical Engineering

Thesis Advisor   Associate Professor Tawatchai Charinpanitkul, D.Eng

Thesis Co-advisor   Professor Wiwut Tanthapanichakoon, Ph.D

       Accepted by the Faculty of Engineering, Chulalongkorn University in Partial Fulfillment of the Requirements for the Master 's Degree

………………………………………….Dean of the Faculty of Engineering
(Professor Direk Lavansiri, Ph.D)

THESIS COMMITTEE

………………………………..…………….. Chairman
(Assistant Professor Vichitra Chongvisal, Ph.D)

………………………………..……….…… Thesis Advisor
(Associate Professor Tawatchai Charinpanitkul, D.Eng)

………………………………………..…….…… Thesis Co-Advisor
(Professor Wiwut Tanthapanichakoon, Ph.D)

……………………………………..……….. Member
(Varong Pavarajarn, Ph.D)

…………………………………..……….. Member
(Soorathep Kheawhom, Ph.D)

กัมปนาท แก้วปลั่ง : การจำลองการเคลื่อนที่แบบ 3 มิติ ของอนุภาคเดี่ยว ตามการไหลแบบ ปั่นป่วนในก๊าซไซโคลนแบบเป่าลง (SIMULATION OF SINGLE PARTICLE MOTION ALONG 3-DIMENSIONAL TURBULENT FLOW IN AIR CYCLONE WITH BLOWDOWN) อาจารย์ที่ปรึกษา: รศ. ดร. ธวัชชัย ชรินพาณิชกุล อาจารย์ที่ปรึกษาร่วม: ศ. ดร. วิวัฒน์ ตัณฑะพานิชกุล จำนวนหน้า 109 หน้า. ISBN 974-17-6026-4.

เครื่องคัดแยกไซโคลนเป็นอุปกรณ์ที่นิยมใช้กันอย่างแพร่หลาย เพื่อแยกหรือคัดขนาด อนุภาคออกจากของไหล การปรับปรุงประสิทธิภาพของไซโคลนให้สามารถดักจับอนุภาคขนาด เล็กกว่าระดับไมครอน กระทำได้โดยการดึงของไหลออกจากส่วนบนของถังเก็บฝุ่น ดังนั้น วัตถุประสงค์หลักของงานวิจัยคือ ศึกษาการเคลื่อนที่ของของไหลและอนุภาคในก๊าซไซโคลน พร้อมทั้งศึกษาผลกระทบของอัตราการเป่าลงต่อประสิทธิภาพการดักจับอนุภาคขนาดเล็กกว่าระดับ ไมครอน และความดันตกคร่อมไซโคลน โดยประยุกต์ใช้วิธีการคำนวณพลศาสตร์ของไหล (CFD) ดังนั้น โปรแกรมเชิงพาณิชย์ FLUENT^{TM} จึงถูกนำมาใช้เพื่อคำนวณการเคลื่อนที่แบบ 3 มิติ ของของ ไหลและอนุภาคในสภาวะการไหลแบบปั่นป่วนในไซโคลน

จากการวิจัยพบว่า ประสิทธิภาพการดักจับอนุภาคและความดันลดที่ได้จากการจำลองมี ความใกล้เคียงเป็นอย่างดีกับผลการทดลองของ Dirgo and Leith (1985) และ Yoshida (1996) โดย การใช้แบบจำลอง Reynolds Stress Model (*RSM)* จะให้ผลการจำลองที่สอดคล้องกับผลการทดลอง มากกว่าการใช้แบบจำลอง $k-\varepsilon$ และ $RNG-k-\varepsilon$ เนื่องจากสมมติฐานของค่าความหนืดปั่นป่วน เป็นแบบนอน-ไอโซทรอปิค ทั้งนี้ ผลการจำลองแสดงให้เห็นว่าการเพิ่มประสิทธิภาพการดักจับ อนุภาคขนาดเล็กกว่าระดับไมครอน สามารถทำได้โดยการเพิ่มความเร็วอากาศ หรือการเพิ่มอัตรา การเป่าลง จากการจำลองพบว่า การเพิ่มความเร็วอากาศจาก 15 เมตรต่อวินาที เป็น 20 เมตรต่อ วินาที จะทำให้ประสิทธิภาพการดักจับอนุภาคขนาด 1.5 ไมครอนเพิ่มขึ้นจาก 6% เป็น 10% และ ความดันลดเพิ่มขึ้น 80% ในขณะที่ การเพิ่มอัตราการเป่าลงเป็น 10% จะสามารถเพิ่มประสิทธิภาพ การดักจับอนุภาคจาก 6% เป็น 21% โดยความดันลดจะเพิ่มขึ้นเพียง 10% เท่านั้น ดังนั้น วิธีการดึง อากาศออกจากถังเก็บฝุ่น จะทำให้เพิ่มประสิทธิภาพการดักจับอนุภาคที่มีขนาดเล็กกว่าระดับ ไมครอน และความดันลดได้ดีกว่าวิธีการเพิ่มความเร็วอากาศขาเข้า

ภาควิชา ....วิศวกรรมเคมี.......... ลายมือชื่อนิสิต ....
สาขาวิชา ....วิศวกรรมเคมี.......... ลายมือชื่ออาจารย์ที่ปรึกษา ………………………………
ปีการศึกษา ....2547................. ลายมือชื่ออาจารย์ที่ปรึกษาร่วม ....

KOMPANART KAEWPLANG: SIMULATION OF SINGLE PARTICLE MOTION ALONG 3-DIMENSIONAL TURBULENT FLOW IN AIR CYCLONE WITH BLOWDOWN. THESIS ADVISOR : ASSOCIATE PROFESSOR TAWATCHAI CHARINPANITKUL, D.Eng. CO-ADVISOR: PROFESSOR WIWUT TANTHAPANICHAKOON, Ph.D., 109 pp. ISBN 974-17-6026-4.

Cyclone separators have been one of the most widely used as equipment for separation or classification of particle from fluid. The improvement of cyclone performance for collecting sub-micron particles can be done by aspirating fluid stream from the upper part of dust hopper. Therefore, the main objectives of this research are to investigate of fluid flow field and particle trajectory within air cyclones and to study the effect of blowdown ratio on the collection efficiency regarding sub-micron particles and pressure drop across cyclones by using Computational Fluid Dynamics (CFD) technique. Therefore, the commercial FLUENT^{TM} program is employed to calculate three-dimensional of fluid dynamics and particle motion with turbulent flow in cyclones.

It can be found in this research that the results of simulation of collection efficiency and pressure drop are good agreement with experimental data of Dirgo and Leith (1985), and Yoshida (1996). The Reynolds Stress Model (*RSM*), non-isotropic turbulent viscosity model, is better agreement with experimental results than the Standard $k - \varepsilon$ and $RNG - k - \varepsilon$ turbulent model. The simulated result shows that to increase collection efficiency of sub-micron particles can be done by increasing inlet air velocity or increasing ratio of blowdown. It can be found in this simulation that increasing inlet air velocity from 15 m/s to 20 m/s, the collection efficiency of particle with 1.5 micron becomes higher from 6% to 10% and the pressure drop also 80% higher. Alternatively, increasing the ratio of blowdown to 10%, the collection efficiency becomes higher from 6% to 21% and the pressure drop is increased only 10%. Therefore, to aspire air from hopper section provides the better collection efficiency and lower pressure drop than increasing inlet air velocity.

Department.....Chemical.engineering...... Student's signature ....

Field of study ..Chemical.engineering..... Advisor's signature ....

Academic year………...2004....…………. Co-advisor's signature ....

ACKNOWLEDGEMENTS

CONTENTS

CONTENTS (continued)

CONTENTS (continued)

LIST OF TABLES

LIST OF FIGURES

LIST OF FIGURES (continued)

LIST OF FIGURES (continued)

NOMENCLATURE

Alphabetical symbols

C Cunningham's slip correction factor

C_D Drag coefficient

$C_{\varepsilon 1}, C_{\varepsilon 2}, C_{\varepsilon 3}$ Constants of turbulent model

F Mass flux

I Turbulent intensity

k Turbulence kinetic energy

ℓ Turbulent length scale

p Pressure

Re   Reynolds number

S_ϕ Source term

Greek symbols

ρ Density

Φ Dissipation function

ϕ General dependent variable

δ_{ij} Kronecker delta function $(\delta_{i=j} = 1, \delta_{i \neq j} = 0)$

μ Dynamic viscosity coefficient

α Under-relaxation factor

μ_t Turbulent viscosity coefficient

τ Viscous stress tensor

Γ Diffusion coefficient

ε Turbulent dissipation energy

κ Von-Karman constant

CHAPTER I

INTRODUCTION

1.1 Motivation

Cyclones are the most widely used air pollution equipment being employed in many kinds of industries for propose of either separating or classifying particulate material from fluid streams. Many industries have paid considerable attention to this kind of unit operation due to its various advantages including simplicity in construction, compactness, low weight and low operating cost. Especially, a compact cyclone has high potential for separating the PM-10 particles.

The flow behavior in the compact cyclone is very complex, especially when the swirl number of fluid dynamics in cylindrical and conical section is high. Semi-empirical or theoretical models are generally employed to explain the complexity of flow pattern within the compact cyclone.

However, such semi-empirical or theoretical model has the limitation. To the best of our knowledge, there is no semi-empirical model taking into account the blowdown ratio for the compact cyclone. The blowdown ratio is the ratio of inlet flow to the outlet flow at the upper region of dust box. Therefore, it is worth to investigate the influence of blowdown ratio on the important variables such as fluid dynamics, particle trajectory, and pressure drop.

Computational Fluid Dynamics or CFD is an analytical tool for systems involving with fluid flow, heat transfer and chemical reaction by computer-base

simulation. In general, velocity, pressure and temperature distribution could be obtained by solving the governing equations of fluid dynamics – the continuity, momentum and energy equations, with assistance of additional equations, which are employed to explain the degree of turbulence. CFD technique can also provide the information of trajectory of disperse phase by using the Newton's second's law.

It should be noted that CFD technique is very helpful for investigating fluid dynamic and particle trajectory, especially, for the system of compact cyclone because its fluid dynamic is too complex to observe experimentally. Moreover, there are several unique advantages of CFD over an experimental approach regarding to the following aspects.

- Disturbance - no probe makes the changing of fluid flow field.
- Information - all variables can be obtained.
- Speed - CFD can perform more speed than experimental investigation.
- Cost - lower of expensive equipments or complicated construction.
- Operating condition - it can easily be conducted at ideal or realistic conditions.

However, it is worth to mention that Computational Fluid Dynamic (CFD) is the complement of theoretical model and experimental investigation. It cannot completely replace the experimental approaches. Computational Fluid Dynamics will help interpret the results of theoretical and experimental investigation.

1.2 Objective

The objectives of this work are to investigate of fluid flow field and particle trajectory within air cyclones and to study the effect of blowdown ratio on the collection efficiency regarding sub-micron particles and pressure drop.

1.3 Scope

The scopes of investigation of fluid dynamic and particle trajectory are:

1. The ratios of blowdown from 0 to 15 %

2. Inlet velocity ranged from 10 to 25 m/s

3. Simulated cyclone with diameter of 4 and 30 cm.

4. Particles with 0.2 - 6 micron in diameter

5. In order to model the turbulence, the standard $k - \varepsilon$, $RNG - k - \varepsilon$, and RSM model are taken into account

CHAPTER II

LITERATURE REVIEWS

Patankar and Spalding (1971) proposed the numerical technique for solving the system of three-dimensional conservation equations for predicting fluid dynamics. The general form of conservation equations including the continuity and momentum equations was solved by finite different method yielding the algebraic equations for the unknown at each grid point. From their research, they applied the staggered grid technique for calculating the gradient of pressure. With this technique, the velocity components were stored between the two pressure nodes. This stagger grid technique avoided the unrealistic phenomena of the momentum equations for oscillating pressures such as the checkerboard pressure field.

Dirgo and Leith (1985) measured the particle collection efficiency and pressure drop of the Stairmand type cyclone at five different flow rates and compared its measurement results with the four theoretical models. The results from Dirgo and Leith (1985) showed that the several theoretical models were underestimated when the inlet velocity was over than 10 m/s. Although, the Barth's model was closest to the experimental result with all range of inlet velocities. For the reason, the assumption of Leith-Licht model, Lapple model, and Dietz model were complete radial back-mixing of uncollected particle. Therefore, a particle was forced to move back into the force vortex region before a particle escaped from the cyclone. In practical phenomena, a particle may return to collide with the cyclone wall.

Kim and Lee (1990) studied on the effect of various variables on the particle collection efficiency; there were the particle size, flow rate, the exit tube size, and cyclone diameter that were taken into account for the nine different geometries. These investigated variables significantly affected on the performance of cyclone because these variables controlled the both of vortexes pattern.

As increasing flow rate, the shape of collection efficiency curve was more stiff due to its tangential velocity was higher. And decreasing the exit tube size increased the cyclone collection efficiency because the region of force vortex (swirling up) was proportional to the size of exit tube. Therefore, the moving down opportunity of a particle was higher.

Moreover, Kim and Lee discussed that the greatest of dimensionless of the exit tube size to the cyclone body size was 0.5. Although, the pressure drop was increased again if this dimensionless was increased over 0.5. Finally, the effect of cyclone body size on the cut size, when the body of cyclone was excessively large then the particle cut size appeared to increase because fluid pattern was changed.

Griffiths and Boysan (1996) calculated the collection efficiency and pressure drop of cyclone. FLUENT^{TM} was the commercial program that was used for simulating the air dynamics within three types of cyclone. The desired cyclones were Aerojet type cyclone, Stairmand's cyclone, and Kim and Lee's cyclone. The calculation results were obtained from solving the conservation equations including continuity equation, momentum equations, and two additional equations. These simulation results were compared with the experimental data and well-known empirical models.

Griffiths and Boysan concluded that the calculation of pressure drop from the $RNG - k - \varepsilon$ model was good agreement with experimental data. The different important assumption between two models was the presence of additional terms in the dissipation rate equation of $RNG - k - \varepsilon$ model. Therefore, in case of high swirling flow, the higher accuracy solution was obtained from $RNG - k - \varepsilon$ model.

Yoshida (1996) investigated the results of circumferential angle, length of moveable guide plate and vertically movable apex cone on cyclone collection efficiency of Iinoya type cyclone. Moreover, The numerical calculation was compared with his experimental result. The calculation results were obtained from the solution of Navier-Stokes equation in three-dimensional with $k - \varepsilon$ model.

The calculation result from Yoshida indicated that the flow field was non-symmetry, the each plane of velocity vector depended on the circumferential angle because the motion characteristic of fluid was spiral. Changing inlet moveable guide plate controlled 50% cut size on 0.45-0.75 micron. However, the cut size was increased again under the condition of very narrow guide plate because fluid turbulent near the guide plate was increased. Finally, 50% cut size also was changed by the vertically apex cone at inlet of dust box.

Huber and Sommerfeld (1998) predicted the fluid dynamics and particle motion in pneumatic conveying with roughness wall. They concerned on numerical calculation using Computational Fluid Dynamics (CFD) technique. This technique was the analysis system of fluid dynamic or heat transfer by solving the conservation equations. In this research, Three-dimensional with $k - \varepsilon$ turbulent model were discretized using the finite volume method for fluid flow calculation. The results of simulation agreed with experimental data from the Phase Doppler Anemometry (PDA) when their algorithm was

    1) Calculation gas flow field without source terms of particle
    2) Solving the equations of motion of disperse phase
    3) Re-calculation fluid dynamics including effect of the source terms
    4) Repetition of step 2 and 3 until the convergence.

Hoekstra, Derksen and Akker (1999) compared the velocity profiles between the experimental data and two mathematical models by using Laser-Doppler Velocimetry (LDV) to measure the axial and tangential velocity for verification with the $k - \varepsilon$ and $RNG - k - \varepsilon$ turbulent models. The fluid flow in compact cyclone was

strongly affected by swirl number; this dimensionless was the ratio of tangential to axial velocity. Hence, they recommended that the Reynolds Stress Model was reasonable agreement with the experimental data and suitable for cyclonic flow more than $k-\varepsilon$ and $RNG-k-\varepsilon$ model. However, the computational time and resource of Reynolds stress transport model was higher than conventional model such as $k-\varepsilon$ model and $RNG-k-\varepsilon$ model.

Ma, Ingham, and Wen (2000) used the $RNG-k-\varepsilon$ turbulence model for the simulation of the highly rotational fluid flow through a group of small cyclone. It should be noted that the standard $k-\varepsilon$ model gave the incorrect fluid velocity because the large turbulent viscosity that is calculated by this model, this model based on the isotropic assumption. Therefore, $RNG-k-\varepsilon$ model was the better reliable model than the standard $k-\varepsilon$ model for investigating on the rotational flow.

The results of Ma et. al. showed that the decreasing size of vortex finder gave rise to a greater difficultly in the particle penetration. And, if the diameter of cyclone body was increased then the distance of wall vortex finder and cyclone wall increased. This reduced the resistance of walls that make the fluid velocity increased. Finally, a particle spent more time in cyclone when it was injected through the top of inlet plane. Therefore, it had the greater chance of separation than the particle was injected at the lower part of inlet plane.

Peng, Boot and Hoffmann (2001) used Laser Doppler Anemometry (LDA) for measuring of the velocity profiles at four different angles including 0°, 90°, 180° and 234°. These positions were located at (i) four detectors in the gas inlet, (ii) one detector in the cylindrical part, and (iii) four detectors in the conical part.

Figure 2.1 shows that the tangential velocity depended on the circumferential angle. It should be note that all the highest peak of tangential velocity located at the vortex finder before it slightly decreased to wall.
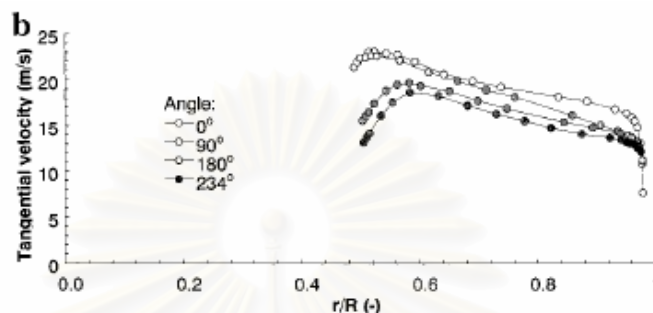
Figure 2.1 Tangential velocity profiles at various circumferential angles

Yoshida, Fukui, Yoshida, and Shinoda (2001) researched on the collection efficiency and pressure drop of the Iinoya's type cyclone, Iinoya's cyclone had double conical section. The solutions of solving three-dimensional Navier-Stokes equations along with $k - \varepsilon$ turbulent model were compared with the experimental results. Yoshida et. al. presented the pressure drop of Iinoya's cyclone that it was 10% lower than the conventional cyclone. However, the experimental pressure drop of the both cyclones was higher than the calculated pressure drop because of the difference of tangential velocity between calculated and experimental. For the experimental collection efficiency of Iinoya's type, the separation efficiency was nearly equal with the conventional cyclone.

Abrahamson, Jones, Lau, and Reveley (2002) studied on the effect of different upstream bends on efficiency of the Stairmand's cyclone. Experimental operation, inlet velocity was 20 m.s^{-1} and solid concentrations was 120 g.cm^{-3}. The reason of changing collection efficiency was explained by the magnitude of the radial velocity of fluid in the free and force vortex. The general discussion in this publication was the cyclone efficiency depended on i) the inlet velocity, ii) the direction of the inlet particle, and iii) the tangential velocity profile of fluid.

Obermair, Woisetschlager, and Staudinger (2003) measured the flow pattern of the three types of outlet tube - dust box, apex cone, or down comer tube. The Laser Doppler Anemometry (LDA) was used for measuring the velocity profiles. This velocity measurement was higher accuracy than a direct measurement because a system was not disturbed.

The collection efficiency of the various types of outlet tube was explained by the fluid dynamics pattern. The cyclone with dust hopper, its efficiency was not good due to the strong secondary flow that was swirling upward direction. By using the apex cone, the separation efficiency was increased because the secondary flow was complete absence. However, Obermair et. al concluded that the best separation efficiency was achieved by changing outlet tube of cyclone with a down comer tube due to the opportunity of particle collision with the outlet wall was increased.

Xiaodong et. al. (2003) investigated the function of turbulent intensity, thickness of boundary layer, and Saffman force on the cyclone's collection efficiency using numerical calculation approach. The one way coupling was taken into account for predicting the particle trajectory in cyclone, only the velocity components of fluid was determined in the equation of fluid phase (without the source term of particle drag force) because the motion of PM10 particles did not change the fluid streamline.

As the turbulence intensity increased, the separation efficiency was decreased. The particle entered to the core region where the direction of axial velocity was upward because of the higher turbulence fluctuation condition. When the thickness of boundary layer was decreased, inner core with a large tangential velocity was enlargement. Therefore, the efficiency was increased because the region of strong centrifugal force on the particles was enlargement. Finally, the Saffman force (the velocity gradient force) effect, this force was not effect on the efficiency when particle diameter larger than 7.5 micron.

Altmeyer et. al. (2004) presented potential of new software for calculating the collection efficiency by using the four empirical models as well as 1) Barth model, 2) Leith and Licht model, 3) Lorenz model, and 4) Mothes and Loffler model. The calculation results at room temperature, Lorenz model and Mothes & Loffler model can predicted very well on the both of cyclone performance that were separation efficiency and cut-size. Alternatively, at the high temperature condition, Leith and Licht model indicated that it estimated the separation efficiency with higher accuracy than another one because this model take into account the temperature effect.

Yang and Yoshida (2004) published the effect of mist injection positions on the particle collection efficiency of 72-mm. cyclone body size. The mist injection position was installed at 180° from the air inlet for increasing the collection efficiency. The simulation result of particle trajectory indicated that the trajectory of the larger particle was near the wall. The large size particle was higher centrifugal force for collision with the cyclone wall. Moreover, the experimental results showed that the collection efficiency could be slightly increased by increasing the ratio of mist to gas. The deposited particles on the wall were wash out by the mist flow. Thus, the mist injection could increase the collection efficiency.

Zhao, Shen, and Kang (2004) studied on the effect of three different types of cyclone inlet. There were A, B and C type – a Conventional Tangential Single Inlet (CTSI) type, a Direct Symmetrical Spiral Inlet (DSSI) type, and a Converging Symmetrical Spiral Inlet (CSSI) type, as shown in **Figure 2.2**. These types of inlet were varied for measuring the collection efficiency and pressure drop across cyclone separator.
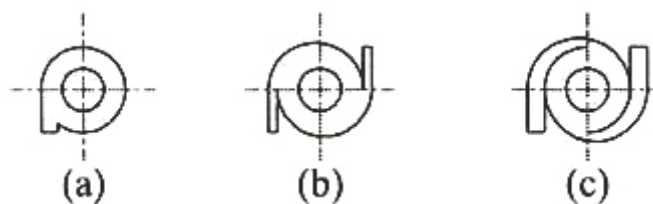
Figure 2.2 The three different types of cyclone inlet

Zhao et. al. described their investigated result that the efficiency significantly increases when ordering was type A, B and C respectively. This result show that injected particles with symmetrical spiral (type B and C) would easily be collected on the wall. Consequently, the pressure drop would be slightly increased with type A, B and C respectively. These indicated that the three types of inlet played an important role on the collection efficiency without increasing the pressure drop significantly.

Gimbun et. al. (2005) concerned on the effect of inlet velocity and temperature by using the simulation approach with FLUENT 6.1 commercial CFD code. The results of CFD technique will be compared with experimental data and four empirical models. Gimbun et. al. concluded that the Reynolds Stress Model (RSM) was the highest potential model for predicting the pressure drop. The maximum deviation was only three percent due to this model can predicted the high swirling and anisotropic flow as well as the fluid dynamics in cyclone. However, The more complicated turbulent model, RSM model, consumed more computational time and its solution was difficult convergence.

CHAPTER III

FUNDAMENTAL KNOWLEDGE

3.1 Cyclone separator

Cyclone separator has been employed in various processes for separation of particulate from fluid flow because it utilizes low energy to create rotational motion of fluid. Moreover, merits of cyclone are inexpensive cost of manufacture, lower maintenance cost, containing no moving part and applicable under high temperature or high pressure.

A general cyclone consists of two parts, which are cylindrical and conical part. Fluid is tangentially injected into cylindrical part before swirls down to the conical section. The detail of fluid flow field in each part will later be shown in section 3.1.1. It should be noted that a conventional cyclone has only an upper outlet pipe of fluid. However, Yoshida (1996) proposed that collection efficiency of a cyclone could be increased when fluid is withdrawn at the lower part of cyclone. The so-called blow-down pipe is an additional outlet that locates at upper section of dust box for increasing collection efficiency or decreasing cut size.

3.1.1 Fluid flow pattern

Fluid tangentially enters to cylinder part before it spins in a vortex and swirls down to the cylinder part. In conical section, the vortex diameter until the flow reverses at the apex of cone and spins up to the vortex finder. Meanwhile, in

cylindrical section, dust particles are centrifuged toward the wall and collected the wall due to centrifugal force. The collected particles flow down to the cone apex, which could result in entrainment of particles from a dust hopper.

A spiral of fluid in the cylindrical part can be divided into three principal components, namely tangential, radial and axial velocity components. Many researchers have attempted to measure the flow dynamics and collection efficiency of cyclone. Dirgo and Leith (1985), Ogawa(1997), and Peng, Boot and Hoffmann (2001) investigated the profiles of velocity component using Phase Doppler Anemometric (PDA) measurement comparing with theoretical models.

Figure 3.1.1 shows the distribution of theoretical velocity components at the various height levels in a commonly used cyclone.

Figure 3.1.1 a) shows the tangential velocity that is the major driving force for particulate classification by using cyclone because this velocity component provides the centrifugal force. The highest peak of this velocity component locates below the vortex finder tube. This velocity profile is a function of cyclone radius as shown in **Equation (3.1.1)**.

$$v_t r^n = \text{Constant} \tag{3.1.1}$$

v_t is tangential velocity, r is radius distance and n is exponent vary from 0.5 to 1 (n = 0 at the boundary of inner and outer vortex).

Figure 3.1.1 b) shows the radial velocity that has two directions. It has positive value when the direction is outward from the center of cyclone. In contrast, its direction is inward as negative sign. It should be noticed that slightly negative values of this velocity component locate in upper region of cyclone. It can be interpreted that the circular zone has occur in this region, it has both or inward and outward direction.

Figure 3.1.1 c) shows the axial velocity component in cyclone separator. The direction of axial velocity in cyclone can be upward or downward. Positive value of this component means its upward direction. In other hand, downward direction has the negative value. The changing point is the separation of free and force vortex region whereas approximates the half of distance between two walls. Many researchers, for instance, Griffiths and Boysan (1996), and Okawa (1997), investigated that axial direction in core region can exhibit the negative value because pressure in this region is low. Therefore, fluid flow field has the back-flow direction when pressure in core region of cyclone is very low.

a)   b)   c)
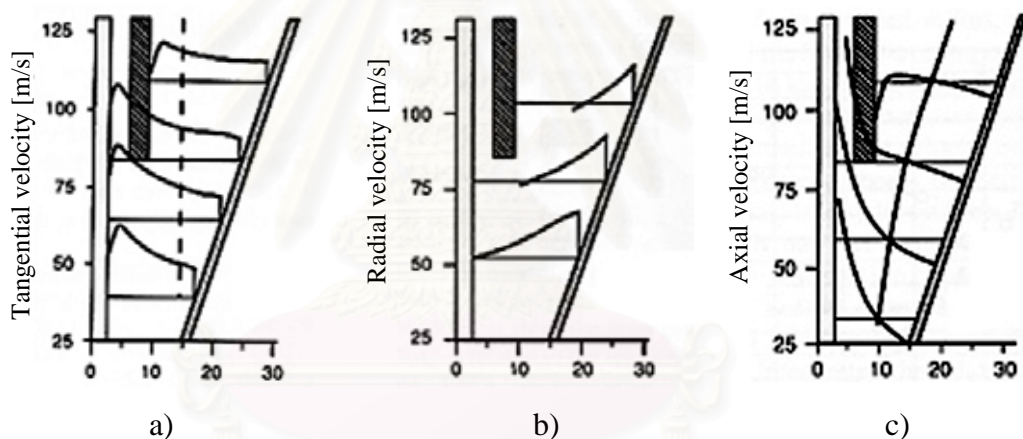
Figure 3.1.1 Distribution of velocity profile in conventional cyclone

3.1.2 The mechanism of particle collection

The particle trajectory within cyclone can be calculated by integrating the equations of particle motion. These equations are based on Newton's second law. The net forces acting on the particle balance with the rate of particle momentum change is called Newton's second law. There are many forces acting on particle in cyclone. However, in practical way those are drag force, centrifugal force and gravity force.

1)   Drag force: when fluid flows pass a spherical particle, drag force will resist for moving of particle therefore its direction always oppose the motion direction. This force depends on the relative velocity between particles to fluid, drag coefficient, fluid density, and cross-sectional area of particle. The relation between many variables and drag force can be shown in **Equation (3.1.2)**.

$$\vec{F}_D = \frac{1}{2}\rho_F A C_D \left(u_F - u_P\right)^2 \qquad (3.1.2)$$

When ρ_F denote the fluid density, A is cross sectional area of particle, u_F and u_P stand for the velocity of fluid and particle, respectively. A drag coefficient (C_D) is the ratio of total momentum transfer of the particle-fluid interface to the momentum transfer by turbulent effect. This coefficient includes the factor of shape, viscosity, compressibility, and boundary layer separation.

2)   Centrifugal force: particle separation is the result of two opposing forces. Not only the centrifugal force acts on particle moving to the wall but also the drag force acts to carry the particles into the axis. However, as the centrifugal force is predominant, a separation takes place. The centrifugal force is subjected occurs to an object that is traveling around center point, which this force tends to move particles away from the center of rotation. The **Equation (3.1.3)** shows the magnitude of this force in linear or angular velocity.

$$\vec{F}_C = \frac{mv^2}{R} = m\omega^2 R \qquad (3.1.3)$$

When v, ω are linear and angular velocities, R is radius of rotational motion.

3)   Gravitational force: the force of gravity is the force which the earth, attracts another smaller object. All objects upon earth have gravity force that is downward direction to the center of the earth. By definition, this force is proportional to the weight of the object as shown in **Equation (3.1.4)**. In the case of high rotational flow

in cyclone, the ratio between centrifugal and gravity force ranges from 100 to 20,000 thus the gravity force is the minor influence for particle collection.

$$\vec{F}_G = m\vec{g} \tag{3.1.4}$$

Where $\vec{g}$ is constant 9.8 [m/s^2] on Earth and m is the mass of object [kg].

Figure 3.1.2 illustrates the two remaining forces acting on the particle that is traced by supplying air in circular path. Centrifugal force is occurred by tangential velocity of fluid and drag force is induced by fluid radius velocity. These forces have the opposite direction. Regarding to the center of vessel, the drag force is inward but the centrifugal force has outward direction. It should be noted that if the inward drag force is larger than the outward centrifugal force, the particle is traced inward direction. In the other hand, particle moves colliding to cyclone wall when centrifugal force has greater than drag force.
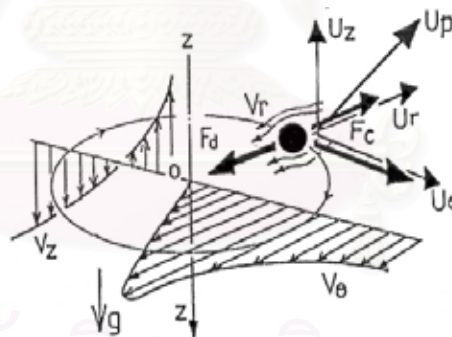
Figure 3.1.2 The direction of important forces

Cyclones are generally classified into four types, depending on how the fluid stream is introduced into cyclone and how the collected particle is discharged. There are four common cyclones that are tangential inlet-axial discharge, tangential inlet-peripheral discharge, axial inlet-axial discharge, and axial inlet-peripheral discharge. However, their operating principles are similar and based on that of the conventional cyclone. The operation theory is based on a vortex motion where the centrifugal force is acting on particle, and particle moves away from the cyclone axis toward to wall.

Figure 3.1.3 shows the both of fluid vortexes within conventional cyclone Particle and air pass tangentially into the cyclone at equal velocities. Particle laden air spirals round the cylinder to create centrifugal force, it swirls in the vortex that include outer and inner vortex. The outer vortex is semi-free vortex, while the inner vortex can be called force vortex. The direction of semi-free vortex is downward with the heavier particle to dust box. On the other hand, the direction of force vortex is upward to the exit pipe. For particle motion, fluid will drag particle moving outward to the cyclone wall. The larger on heavier particles rapidly stick to the outside wall and they move swirling down to dust box. The smaller or lighter particle and clean air spiral upward direction along the centre axis of cyclone and passes out to the vortex finder.
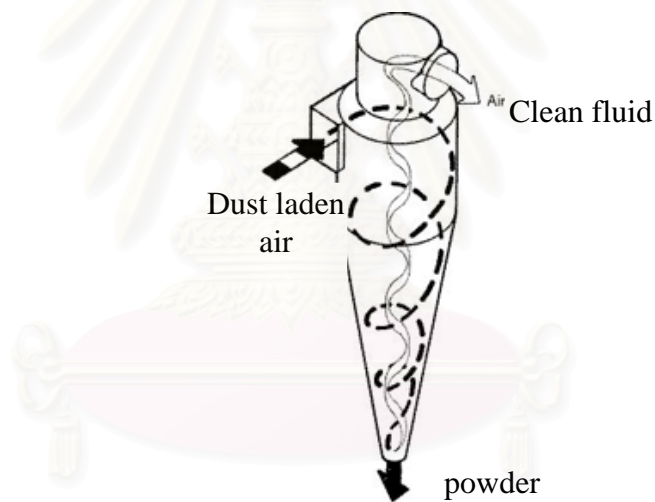
Figure 3.1.3 Free and force vortex within tangential inlet cyclone

3.1.3 Cyclone collection efficiency

The collection efficiency and pressure drop are the major parameters for evaluating the cyclone performance. The definition of cyclone efficiency is its ability to capture and retain dust particles whereas the pressure drop is the amount of power that the unit needs to process. For any given cyclone it is desirable to have as high collection efficiency and low pressure drop as possible. Unfortunately, changes in design or operating variables that induce to increase collection efficiency also tend to increase pressure drop. Higher efficiency cyclone comes with higher-pressure drop, which require higher energy cost for separating particle from fluid stream.

The cyclone collection efficiency is dependent on many factors, for instance, the design of cyclone dimensions, the properties of the gas and particle, the amount of dust contained in gas, and particle size distribution etc. The collection efficiency curve is obtained by experimenting on a specific cyclone. In other alternative, many empirical models for predicting cyclone collection efficiency have been presented by different investigators. There are commonly used empirical models for calculating collection efficiency of cyclone, for instance, Barth (1956) model, and Iozia and Leith (1989) model. The investigated results of Griffiths and Boysan (1996) also showed that only the empirical model of Iozia and Leith (1989) had been shown to be useful in experimental performance for Stairmand's type cyclone.

For Barth's (1956) empirical model, the height of cylindrical core, h*, is related to the geometric parameters,

$$h* = \begin{cases} H - S & De \leq B \\ \dfrac{(H-h)(D-D_e)}{(D-B)} + (h-S) & De > B \end{cases} \qquad (3.1.5)$$

The swirling component of the fluid velocity at the edge of the cylindrical core of the cyclone is v_t.

$$v_t = v_{in} \left[\frac{(De/2)(D-b)\pi}{2ab\alpha + h*(D-b)\lambda\pi} \right]$$

(3.1.6)

Whereas a, b are the height, width of inlet pipe, respectively. D, D_e are the body size of cyclone and diameter of exit tube, respectively. Finally, the wall friction coefficient (λ) is assumed 0.02 and $\alpha = 1 - 1.2(b/D)$.

Terminal velocity of a particle in cyclone can be determined by **Equation (3.1.7)**. When Q is defined as the volumetric gas flow rate in the cyclone.

$$\frac{v_{ts}}{v_{ts}^*} = \frac{\pi h * v_t^2 \rho_p \phi^2}{9\mu Q}$$

(3.1.7)

Barth (1956) concluded that the particle collection efficiency of a cyclone was best described by using a function of the particle terminal settling velocity. This collection efficiency can be expressed in **Equation (3.1.8)**.

$$\eta = \frac{1}{1 + \left(\frac{v_{ts}}{v_{ts}^*}\right)^{-3/2}}$$

(3.1.8)

Many researchers have contributed the publications to improve cyclone collection efficiency and pressure drop. For instance, Dirgo and Leith (1985), Kim and Lee (1990), Griffiths and Boysan (1996), and Hoekstra et. al. (1999) described the effect of the inlet velocity of fluid on the collection efficiency. Moreover, Patterson (1996), Yoshida (1996), Ogawa (1997), Obermair et. al. (2003), and Zhao et. al. (2004) studied the effects of cyclone dimensions and operating conditions of cyclone on the collection efficiency. The important parameter can be summarized in **Table 3.1.1**.

Table 3.1.1 Effect of parameters on cyclone efficiency

Parameter	Change	Effect on efficiency
Pressure drop	Increase	Increase
Flow rate	Increase	Increase
Particle size	Increase	Increase
Viscosity	Increase	Decrease
Solid concentration	Increase	Decrease
Cyclone diameter	Increase	Decrease
Vortex finder length	Increase	Decrease

3.1.4 Pressure drop across a cyclone

A common cyclone separator uses the centrifugal force to separate particulate matter from the fluid stream. The dust-laden air stream enters tangentially at the top of cyclone and moves down to the lower section of cyclone. When the fluid reaches to the bottom of cyclone, the gas flow will reverse into inner vortex. The velocity components in the both of vortexes consist of tangential velocity, radial velocity and axial velocity. It should be noted that the tangential velocity is the dominant velocity component for calculating the pressure drop. The relation between tangential velocity and pressure profile can be expressed in **Equation (3.1.9)**, which the pressure distribution varies with the radius position in a cyclone.

$$\frac{dP}{dr} = \rho \frac{V_t^2}{r} \tag{3.1.9}$$

Figure 3.1.4 shows the pressure and tangential velocity distribution within a common cyclone. It can be seen that the highest pressure is located at the wall of the cyclone. The pressure decreases with the reduction of the radius position because of the increasing tangential velocity. In the radial direction, there is a significant pressure drop caused by the change of the tangential velocity. This pressure change in the radial direction can be expressed by the above **Equation (3.1.9)**. However, according to Peng et. al. (2001), and Yoshida (1996) the velocity profile and pressure distribution might not be symmetry because of the swirling flow of fluid in cyclone.
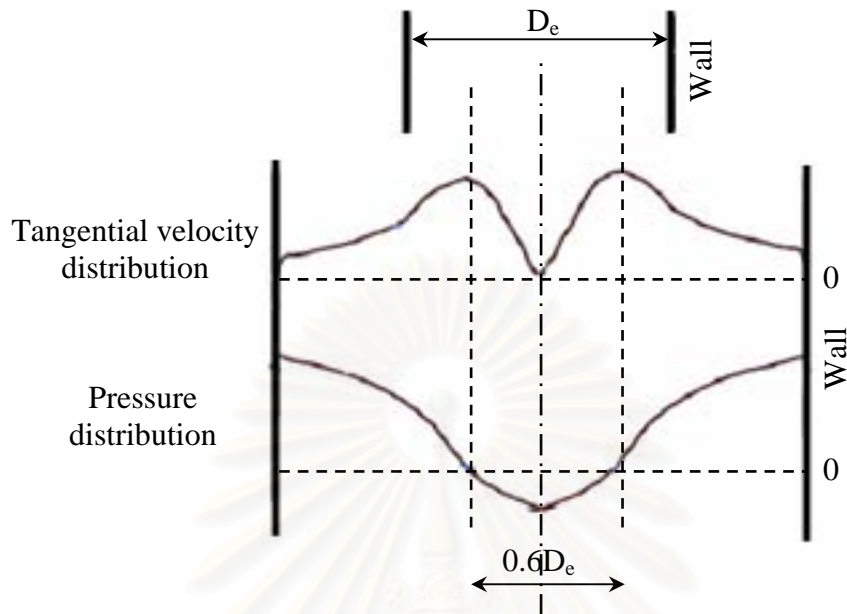
Figure 3.1.4 Pressure and tangential velocity distribution

The pressure drop over a cyclone is a function of the cyclone dimensions and its operating conditions. Shepherd and Lapple (1939) determined the optimum dimensions of cyclones based on the body diameter. There are many factors affecting the pressure drop across the cyclone: the wall friction, the changing of flow direction, the sudden enlargement at inlet pipe or sudden contraction at the vertex finder, and the fluid viscosity effect. However, it is well known that the pressure drop is proportional to square of the inlet velocity as shown in **Equation (3.1.10)**.

$$\Delta P = N \frac{\rho \, v_{inlet}^2}{2} \tag{3.1.10}$$

The pressure drop coefficient (N) in **Equation (3.1.10)** includes the pressure drop due to force vortex, sudden enlargement and sudden contraction. There are the two suitable models are employed in this research. The model of Shepherd and Lapple, and Coker's model are listed in **Table 3.1.2**.

Table 3.1.2 The empirical models of pressure coefficients (N)

Model	N
Shepherd and Lapple model	$16\dfrac{ab}{D_e^2}$
Coker model	$9.47\dfrac{ab}{D_e^2}$

All notations of cyclone dimensions for these two empirical models of pressure coefficients are shown in **Figure 3.1.5**.
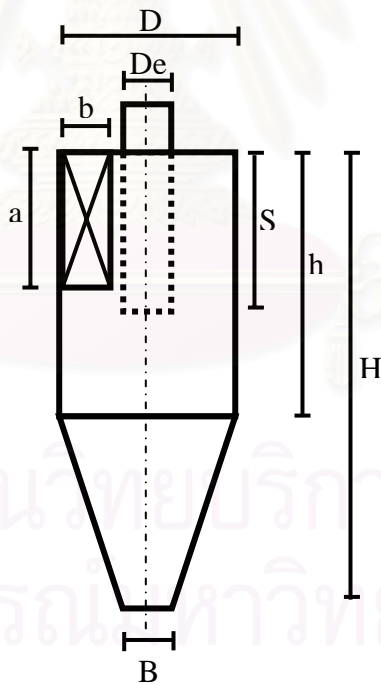
Figure 3.1.5 The notations of conventional cyclone dimensions

3.1.5 Advantage and disadvantage of cyclone separator

Many processes in chemical industrials require the particle separation. There are various equipments for this objective but cyclone has the advantages over the other particulate collection device that are shown in **Table 3.1.3**.

Table 3.1.3 Advantage and disadvantage of cyclone separator

Advantages	- No moving parts and minimum space requirements - Easy to install and replace defective parts - Service conditions of temperature, dust loading, erosion - Removing liquids from gas - Low capital and maintenance costs
Disadvantages	- Lower collection efficiency - Higher collection efficiencies only at high pressure drops - Medium to high operating costs

3.2 Numerical approach for fluid phase

3.2.1 Equations of mass and momentum conservation

The principal Equations of fluid dynamics are derived from the conservation laws, the conservation of mass, momentum and energy. All of the conservation equations describe the net quantities across the boundary are conservation, while the amount of the quantity crossing the boundary, flux, consists of two parts: one is the convective transport and the different flux is the diffusion flux. FLUENT can solve basically equations of mass, momentum and energy conservation. For flows involving heat transfer or compressibility, an additional equation for energy conservation is also taken into account. For flows involving species mixing or reactions, equation of conservation of each species also considered. If the non-premixed combustion model is used, conservation equations for the mixture fraction and its variance are solved. Additional transport equations are also solved when the flow is turbulent.

Mass conservation equation

The first step to obtain mass conservation equation is to write down a mass balance, which is based on the fact that means the mass cannot increase or disappears from the desired system.

> Rate of increase of mass   =   Net rate of flow of
> in fluid element   mass into fluid element

The equation of mass conservation can be written in the partial differential equation form as shown in **Equation (3.2.1)**. The first term on the left hand side is the rate of change in time of the density (mass per unit volume). The second term describes the net flow of mass out of the element across its boundaries. For an incompressible fluid, the density is constant. Therefore, the **Equation (3.2.1)** becomes **Equation (3.2.2)**.

$$\frac{\partial \rho}{\partial t} + div(\rho \vec{u}) = 0 \tag{3.2.1}$$

$$div(\rho \vec{u}) = \frac{\partial u}{\partial x} + \frac{\partial v}{\partial y} + \frac{\partial w}{\partial z} = 0 \tag{3.2.2}$$

Whereas ρ and t denote the density of fluid and time, $\vec{u}$ is the velocity vector.

Momentum conservation equations

The conservation of momentum equations are derived from Newton's second law. The Newton's second law explains that the net force acting on an element equal to mass time acceleration. However, the acting force can be classified as two main types, which are body force and the surface force. Body force directly acts on the mass of the volume (gravitational, buoyancy, Coriolis or centrifugal forces). Surface force directly acts on the surface (pressure, shear or normal stresses). It should be noted that the effect of body force is included as source term, while the surface force will calculate as separate terms.

Table 3.2.1 summarizes the conservation form of the system of equations. The governing equations are the unsteady state of three-dimensional fluid flow of a compressible Newtonian fluid. It can be called Navier-Stokes equations.

Table 3.2.1 Summarization of the momentum conservation equations

x-momentum	$\frac{\partial \rho u}{\partial t} + div(\rho u \vec{u}) = -\frac{\partial P}{\partial x} + div(\mu \, grad(u)) + S_{\phi x}$
y-momentum	$\frac{\partial \rho v}{\partial t} + div(\rho v \vec{u}) = -\frac{\partial P}{\partial y} + div(\mu \, grad(v)) + S_{\phi y}$
z-momentum	$\frac{\partial \rho w}{\partial t} + div(\rho w \vec{u}) = -\frac{\partial P}{\partial z} + div(\mu \, grad(w)) + S_{\phi w}$

3.2.2 Turbulence

The nature of turbulent flow, chaotic and random state of motion, and the physics of transition from laminar to turbulent flow cannot be represented by Narvier-Stoke equations because the velocity fluctuations give rise to additional stress on fluid, which is called Reynolds stresses. These fluctuations mix transported quantities such as momentum, energy, and species concentration. To investigate the effect of fluctuation, the summation of mean and fluctuation components are replaced into Narvier-Stoke equations before the time average is taken applying. Consequence, Narvier-Stoke equations become the set of Reynolds-Average Navier-Stoke equations (RANS as shown in **Table 3.2.2**.

Table 3.2.2 The set of Reynolds-Average Navier-Stoke equations (RANS)

Continuity equation

$$\frac{\partial \rho}{\partial t} + div(\bar{\mathbf{U}}) = 0$$

Reynolds equations

$$\frac{\partial \rho U}{\partial t} + div(\rho U\bar{\mathbf{U}}) = -\frac{\partial P}{\partial x} + div(\mu \, grad(U)) + \left[-\frac{\partial(\rho \overline{u'^2})}{\partial x} - \frac{\partial(\rho \overline{u'v'})}{\partial y} - \frac{\partial(\rho \overline{u'w'})}{\partial z} \right]$$

$$\frac{\partial \rho V}{\partial t} + div(\rho V\bar{\mathbf{U}}) = -\frac{\partial P}{\partial y} + div(\mu \, grad(V)) + \left[-\frac{\partial(\rho \overline{u'v'})}{\partial x} - \frac{\partial(\rho \overline{v'^2})}{\partial y} - \frac{\partial(\rho \overline{v'w'})}{\partial z} \right]$$

$$\frac{\partial \rho W}{\partial t} + div(\rho W\bar{\mathbf{U}}) = -\frac{\partial P}{\partial z} + div(\mu \, grad(W)) + \left[-\frac{\partial(\rho \overline{u'w'})}{\partial x} - \frac{\partial(\rho \overline{v'w'})}{\partial y} - \frac{\partial(\rho \overline{w'^2})}{\partial z} \right]$$

Scalar transport equation

$$\frac{\partial \rho \phi}{\partial t} + div(\rho \phi \bar{\mathbf{U}}) = div(\mu \, grad(\phi)) + \left[-\frac{\partial(\rho \overline{u'\phi'})}{\partial x} - \frac{\partial(\rho \overline{v'\phi'})}{\partial y} - \frac{\partial(\rho \overline{w'\phi'})}{\partial z} \right]$$

The nine fluctuation components can be written in Reynolds stresses.

Normal Reynolds stress: $\qquad \tau_{xx} = -\rho\overline{u'^2}$, $\quad \tau_{yy} = -\rho\overline{v'^2}$, $\quad \tau_{zz} = -\rho\overline{w'^2}$

Shear Reynolds stress: $\qquad \tau_{xy} = \tau_{yx} = -\rho\overline{u'v'}$, $\tau_{xz} = \tau_{zx} = -\rho\overline{u'w'}$, $\tau_{yz} = \tau_{zy} = -\rho\overline{v'w'}$

All Reynolds stresses appear on the right hand side of the RANS equation, which these terms are proportional to the rate of deformation of fluid element. It should be note that all Reynolds stress terms are an analogy on the viscous stresses. Boussinesq (1877) proposed that Reynolds stresses could be linked to mean rates of deformation. **Equation (3.2.3)** is an extended Boussinesq equation, which is used for computing the Reynolds stresses in $k - \varepsilon$ model.

$$\tau_{ij} = -\rho\overline{u_i'u_j'} = \mu_t(\frac{\partial u_i}{\partial x_j} + \frac{\partial u_j}{\partial x_i}) - \frac{2}{3}\delta_{ij}k \qquad (3.2.3)$$

For most applications it is unnecessary to solve the detail of turbulent fluctuations. Only the effects of turbulence on the mean flow are taken into account. There are several turbulent models to describe the turbulent phenomena but high potential of turbulent models should have wide applicability, accuracy, simple and economic to run. The common used turbulent models are shown in **Table 3.2.3**.

Table 3.2.3 The division of turbulence models

Classical model	Base on (time-average) Reynolds equations
	1. Zero equation model – mixing length model
	2. Two equations - $k - \varepsilon$ model
	3. Reynolds stress model
	4. Algebraic stress model
Large eddy simulation	Base on time-independent flow equations

Table 3.2.4 describes the behavior and usage of all models that are applied for predicting fluid flow within cyclone in this research. All turbulent models have advantages and limitations for predicting the turbulent flow regime. For example, the $standard - k - \varepsilon$ model is the simplest turbulent model for many industrial relevant flows, while it has poor performance for important case such as rotation flow, separation or counter flow.

Table 3.2.4   The behavior and usage of RANS turbulence models

Model	Behavior and usage
$standard - k - \varepsilon$	The baseline two transport equation model solving for k and ε. The coefficients are empirically derived; valid for fully turbulent flows only. Option to account for viscous heating, buoyancy Widely used despite the known limitations of model. Performs poorly for complex flow involving separation, strong rotational flow, Suitable for initial iterations
$RNG - k - \varepsilon$	A variant of the $standard - k - \varepsilon$ model. Equations and its coefficients are analytically derived. Significant changes in the ε equation improves the ability to model highly rotational flow. Additional options aid in predicting swirling and low Reynolds number. Suitable for complex shear flows involving rapid strain, moderate swirl, vortices, and locally transition flows
RSM	Reynolds stresses are solved directly with transport equations avoiding isotropic viscosity assumption of other models. Avoid isotropic eddy viscosity assumption. More CPU time and memory is required. Tougher to converge due to close coupling of equations. Suitable for complex 3D flows with strong streamline curvature, strong swirl/rotation e.g. cyclone.

3.2.3 Discretization method: Finite volume method

FLUENT is a commercial program that this research uses. This commercial code is a computational fluid dynamics (CFD) program widely employed within many types of industry. It uses the finite volume technique for converting the partial differential equations to the algebraic equations by replacing the continuous values of differential equations with discrete points. However, the discretization methods for converting the partial differential equations consist of three approaches. All of the discretization methods are finite difference method, finite element method and finite volume method. It should be noted that the first and second method are not shown in detail. The detail of these methods are written in many textbooks as Patankar [1980], Versteeg [1995], Ferziger et. al. [1999], Blazek [2001] or Chung [2002]

McDonald et. al. [1971] is the first group who employed the finite volume for calculation of transonic problem. The finite volume method has the easily method for calculating fluid dynamics in complex geometry when comparing with finite difference method because the coordinate transformation is not required. Hence, many publications in field of CFD have used this technique for predicting the properties of fluid and its dynamics.

The attractive of this finite volume method is principle of physical conservation. The control volume integration of the finite volume method is the difference process from the other ones. The finite volume method is originally developed as a special finite difference formulation. The numerical algorithm consists of the following steps:

- Integrate the governing equations over the control volumes.
- Substitute the approximation derivative terms. This process converts the equations into a system of algebraic equations.
- Solve the algebraic equations by an iterative method.

3.2.4 SIMPLE method

The SIMPLE algorithm (Semi-Implicit Method for Pressure-Linked Equations) is a most widely iterative algorithm in computational fluid dynamics. Patankar and Spalding (1972) introduced this method for solving partially incompressible fluid flow. SIMPLE method is the pressure-base method that introduces pressure into continuity equation for calculation a pressure correction field. If the corrected pressure and velocities were added in the momentum equations for calculating the actual velocities, the mass is conservation.

The algorithm of SIMPLE method can be described by the following step and shown in **Figure 3.2.1**.

1) Guess the pressure p^* at each nodal point.

2) To solve the momentum equations for determining the guessed velocity components such as u^*, v^* and w^*.

3) To solve the pressure-correction equations, the modified pressures (p') are obtained at each point.

4) To calculate the corrected pressure and velocities,

$$p_{i,j,k} = p^*_{i,j,k} + \alpha p'_{i,j,k} \text{ and } u_{i,j,k} = u^*_{i,j,k} + d_{i,j}(p' - p')$$

5) When α and d_{ij} are denoted the under-relaxation and ratio of the cross sectional area to coefficients (a_{ij}).

6) To check the convergence by substitution all of the corrected velocity components $(u_{i,j,k}, v_{i,j,k}, w_{i,j,k})$ into the continuity equation. If the residual is equal or less than the tolerance, the program will terminate.

7) To replace the guessed values (p^*, u^*, v^*, w^*) with the corrected values (p, u, v, w) before resolving into step 3.

Guess pressure (p^*)
Initial velocities (u^*, v^*, w^*)

To solving the equations of momentum with TDMA

$$a_{i+1,j,k}u^*_{i+1,j,k} = \sum a_{nb}u^*_{nb} - (A_{i+1,j,k}p^*_{i+1,j,k} - A_{i,j,k}p^*_{i,j,k}) + \overline{S}_\phi \Delta V_u$$

$$a_{i,j+1,k}v^*_{i,j+1,k} = \sum a_{nb}v^*_{nb} - (A_{i,j+1,k}p^*_{i,j+1,k} - A_{i,j,k}p^*_{i,j,k}) + \overline{S}_\phi \Delta V_v$$

$$a_{i,j,k+1}w^*_{i,j,k+1} = \sum a_{nb}w^*_{nb} - (A_{i,j,k+1}p^*_{i,j,k+1} - A_{i,j,k}p^*_{i,j,k}) + \overline{S}_\phi \Delta V_w$$

u^*, v^*, w^*

To solving the pressure correction equation for $p'_{i,j,k}$

$$a_{i,j,k}p'_{i,j,k} + a_{i+1,j,k}p'_{i+1,j,k} + a_{i-1,j,k}p'_{i-1,j,k} + a_{i,j+1,k}p'_{i,j+1,k}$$
$$+ a_{i,j-1,k}p'_{i,j-1,k} + a_{i,j,k+1}p'_{i,j,k+1} + a_{i,j,k-1}p'_{i,j,k-1} + c'_{i,j,k} = 0$$

$p'_{i,j,k}$

Modification all unknowns

$$p_{i,j,k} = p^*_{i,j,k} + p'_{i,j,k}$$

$$u_{i+1,j,k} = u^*_{i+1,j,k} - d_{i+1,j,k}(p'_{i+1,j,k} - p'_{i-1,j,k})$$

$$v_{i,j+1,k} = v^*_{i,j+1,k} - d_{i,j+1,k}(p'_{i,j+1,k} - p'_{i,j,k})$$

$$w_{i,j,k+1} = w^*_{i,j,k+1} - d_{i,j,k+1}(p'_{i,j,k+1} - p'_{i,j,k})$$

$u^* = u$
$v^* = v$
$w^* = w$

No

$$A\left[u_{i+1,j,k} - u_{i,j,k}\right] + A\left[v_{i,j+1,k} - v_{i,j,k}\right]$$
$$+ A\left[w_{i,j,k+1} - w_{i,j,k}\right] \le tolelance$$

Yes

Stop

Figure 3.2.1 SIMPLE algorithm

3.3 Numerical approach for particle motion

3.3.1 Particle trajectory

The particle trajectory can be calculated by using integration over time to the equation of particle motion. The result of this procedure is trajectory of particle in fluid phase. This procedure is adequate when the discrete phase is present at a low mass and momentum loading, in which case the continuous phase is not impacted by the presence of the discrete phase. Moreover, particle-particle interaction is also neglect. For the one-way coupling calculation, there are following steps:

1. Solving the fluid flow filed without source terms of particle phase.
2. Solving the particle trajectory by using fluid flow field at step 1.
3. Re-calculation fluid dynamics including effect of the source terms
4. Repetition of step 2 and 3 until the convergence.

CHAPTER IV

MATHEMATICAL MODEL AND INVESTIGATED SYSTEM

4.1 Governing equations of fluid dynamics

It is the fact that no single turbulence model is universally accepted for all turbulence problems. The choice of turbulence model will depend on considerations; the class of physical problem, the level of accuracy, the computational time. There are many models in FLUENT program to predict fluid dynamics with turbulent effect. The fluid dynamics when turbulent effect is taken into account. However, we choose three models that are Standard $k - \varepsilon$ (SKE) model, $RNG - k - \varepsilon$ ($RNG - k - \varepsilon$) model and Reynolds Stress Model (RSM) because they can give the adequate accuracy of solution with appropriate computational effort.

In according to section 3.2.2, the sets of RANS describe the fluid flow with turbulent effect, including the continuity and momentum equations in tensor notation. These additional terms, Reynolds Stresses ($-\overline{u_i' u_j'}$), must be modeled by using the three turbulent models as mention above to substitute in **Table 4.1.1**.

Table 4.1.1 Reynolds-Averaged Narvier-Stokes (RANS) equations

Continuity equation
$$\frac{\partial \rho}{\partial t} + \frac{\partial}{\partial x_i}\left(\rho u_i\right) = 0$$
Momentum equations
$$\frac{\partial}{\partial t}\left(\rho u_i\right) + \frac{\partial}{\partial x_j}\left(\rho u_i u_j\right) = -\frac{\partial P}{\partial x_i} + \frac{\partial}{\partial x_j}\left[\mu\left(\frac{\partial u_i}{\partial x_j} + \frac{\partial u_j}{\partial x_i}\right)\right] + \frac{\partial}{\partial x_j}\left(-\overline{u_i' u_j'}\right) + S_\phi$$

4.1.1 Standard $k - \varepsilon$ model (SKE)

Launder and Spalding (1974) proposed Standard $k - \varepsilon$ model to predict the turbulent fluid flow. This model is wildly used in many fluid applications because it consumes less computational time and resource. However, if high swirling flow is concerned, this SKE model should be avoid. Because its model do not taken into account the effect of high rotational flow.

The common mathematical model for solving the Reynolds Stresses ($-\overline{u'_i u'_j}$) in this SKE model is employed the Boussinesq hypothesis, the extend Boussinesq equation is relation with mean velocity gradient as **Equation (4.1.1)**.

$$-\rho \overline{u'_i u'_j} = \mu_t \left(\frac{\partial u_i}{\partial x_j} + \frac{\partial u_j}{\partial x_i} \right) - \frac{2}{3} \rho k \delta_{ij} \qquad (4.1.1)$$

According to the **Equation (4.1.1)**, additional turbulent kinetic energy (k) is modeled to substitute. The standard $k - \varepsilon$ (SKE) model is a semi-empirical model bases on the transport equations for turbulent kinetic energy (k) and its rate of dissipation (ε). The model of transport equation for k is derived from the exact equation, while the model of transport equation for ε is obtained using physical reasoning. These two equations are written in **Equation 4.1.2** - **4.1.3**, respectively.

$$\frac{\partial}{\partial t}(\rho k) + \frac{\partial}{\partial x_i}(\rho k u_i) = \frac{\partial}{\partial x_j}\left[\left(\mu + \frac{\mu_t}{\sigma_k} \right) \frac{\partial k}{\partial x_j} \right] + \left(G_k + G_b \right) - \left(\rho \varepsilon + Y_M \right) + S_k \qquad (4.1.2)$$

$$\frac{\partial}{\partial t}(\rho \varepsilon) + \frac{\partial}{\partial x_i}(\rho \varepsilon u_i) = \frac{\partial}{\partial x_j}\left[\left(\mu + \frac{\mu_t}{\sigma_\varepsilon} \right) \frac{\partial \varepsilon}{\partial x_j} \right] + C_{\varepsilon 1} \frac{\varepsilon}{k}(G_k + C_{\varepsilon 3} G_b) - C_{\varepsilon 2} \rho \frac{\varepsilon^2}{k} + S_\varepsilon \qquad (4.1.3)$$

For the four constants, these $C_{\varepsilon 1}$, $C_{\varepsilon 2}$, σ_k and σ_ε are obtained by data fitting.

$$C_{1\varepsilon} = 1.44, \quad C_{2\varepsilon} = 1.92, \quad \sigma_k = 1.0 \text{ and } \quad \sigma_\varepsilon = 1.0 \qquad (4.1.4)$$

In word, the equations are

| Rate of change of k or ε | + | Transport of k or ε by convection | = | Transport of k or ε by diffusion | + | Rate of production of k or ε | - | Rate of destruction of k or ε | + | Source terms |

The turbulent or eddy viscosity that appears in **Equation (4.1.2) – (4.1.3)**, which is derived by production of turbulent velocity scale (ϑ) = $k^{\frac{1}{2}}$ and length scale (ℓ) = $\dfrac{k^{\frac{3}{2}}}{\varepsilon}$ with C_μ is the dimensionless constant of proportionality, can be shown in **Equation (4.1.5)**.

$$\mu_t = f\left(\rho\frac{k^2}{\varepsilon}\right) = \rho C_\mu \frac{k^2}{\varepsilon} \tag{4.1.5}$$

The definition of G_k is the production of turbulence kinetic energy due to the mean velocity gradients. It should be mention that this term is similarly modeled for SKE and also $RNG - k - \varepsilon$ model. It is shown in **Equation (4.14)**, while S_{ij} is strain rate.

$$G_k = 2\mu_t S_{ij} S_{ij} \tag{4.1.6}$$

To identify that G_b in **Equation (4.1.3)** is the production of turbulence kinetic energy due to buoyancy. A default value of turbulent Prandtl number ($\Pr_t$) is 0.85.

$$G_b = -g_i \frac{\mu_t}{\Pr_t}\frac{\partial \rho}{\partial x_i} \tag{4.1.7}$$

Next, Y_M is neglected because Mach number in cyclone is lower than one means. This term is called dilatation dissipation, the effect of compressibility on turbulence fluid flow. This assumption will be described in detail in section 4.4.

4.1.2 The $RNG - k - \varepsilon$ **model (** $RNG - k - \varepsilon$ **)**

The $RNG - k - \varepsilon$ model has almost similar form to the standard $k - \varepsilon$ model. The $RNG - k - \varepsilon$ turbulence model is derived from the instantaneous Navier-Stokes equations, using a statistical technique called "renormalization group" (RNG). The derivation of this model has slightly difference from SKE model. The major differences of this model with the SKE model are the method of calculation turbulent viscosity, the additional term to include the rotational effect in the ε equation.

The additional terms and function in the $RNG - k - \varepsilon$ models of its ε equation that significant improves the accuracy for more many applications, for instance, complex shear flow, flow with high strain rate, swirl and separation flow. The effect of swirl on turbulence is included in this model therefore this model has more accuracy solution for swirling flow than previous model. In short, these features make the $RNG - k - \varepsilon$ model more accuracy for a wider class of flows than the SKE model.

The extend Boussinesq equation to solve the Reynolds Stresses ($-\overline{u_i' u_j'}$) in SKE model is also employed; it can be shown in **Equation (4.1.8)**. Advantage of this approach is low computational effort when it is compared with RSM turbulent model. In contrast, disadvantage of Boussinesq equation is that it assumes μ_t is an isotropic.

$$-\rho \overline{u_i' u_j'} = \mu_t \left(\frac{\partial u_i}{\partial x_j} + \frac{\partial u_j}{\partial x_i} \right) - \frac{2}{3} \rho k \delta_{ij} \tag{4.1.8}$$

The transport equations of k and ε for the $RNG - k - \varepsilon$ model can be shown in **Equation (4.1.9) - (4.1.10)**.

$$\frac{\partial}{\partial t}(\rho k) + \frac{\partial}{\partial x_i}(\rho k u_i) = \frac{\partial}{\partial x_j}\left[\alpha_k \mu_t \frac{\partial k}{\partial x_j} \right] + G_k + G_b - \rho \varepsilon - Y_M + S_k \tag{4.1.9}$$

$$\frac{\partial}{\partial t}(\rho \varepsilon) + \frac{\partial}{\partial x_i}(\rho \varepsilon u_i) = \frac{\partial}{\partial x_j}\left[\alpha_\varepsilon \mu_t \frac{\partial \varepsilon}{\partial x_j} \right] + C_{1\varepsilon} \frac{\varepsilon}{k}(G_k + C_{3\varepsilon} G_b) - C_{2\varepsilon} \rho \frac{\varepsilon^2}{k} - R_\varepsilon + S_\varepsilon \tag{4.1.10}$$

While G_k, G_b and Y_M are exactly similar with the previous SKE model.

The difference of $RNG - k - \varepsilon$ model and standard $k - \varepsilon$ model is the additional quantities of α_k and α_ε, which are called the inverse of Prandtl numbers. The default values of α_k and α_ε are similarly approximated to 1.393.

The important difference term of this model can be seen that R_ε in **Equation (4.1.10)**. The $RNG - k - \varepsilon$ model provides an option to account the additional effect; the effects of swirling or rotational flow. It is the additional effect, which can be shown in **Equation (4.1.11)**.

$$R_\varepsilon = \frac{C_\mu \rho \eta^3 \left(1 - \eta/\eta_0\right)}{1 + \beta \eta^3} \frac{\varepsilon^2}{k} \qquad (4.1.11)$$

The model of turbulent viscosity in $RNG - k - \varepsilon$ turbulent model is included the rotational effect. The modified turbulent viscosity is seen in **Equation (4.1.12)**. This modified model is better accuracy than SKE model because it is taken into account not only old turbulent viscosity that similarly from SKE model but also swirl number.

$$\mu_t = \mu_{t,SKE} \cdot f\left(\alpha_S, S, \frac{k}{\varepsilon}\right) \qquad (4.1.12)$$

It should be mention from **Equation (4.1.12)** that $\mu_{t,SKE}$ is calculated from the **Equation (4.1.5)** of previous SKE turbulent model and the default value of swirl constant (α_S) is set to 0.05, and S is the swirl number that FLUENT recommends 0.5 for strong swirl flow.

Finally, the model constants in **Equation (4.1.10) - (4.1.12)** have derived also analytically by the RNG theory, the defaults are $C_{1\varepsilon} = 1.42$, $C_{2\varepsilon} = 1.68$, $C_\mu = 0.0845$.

4.1.3 The Reynolds Stress Model (RSM)

RSM turbulent model is the clearly complex, but it is the generally accepted that they are the simplest type of model with the potential to describe all the mean flow properties. This model consumes very large computational cost for calculating of six partial differential equations for individual Reynolds stresses ($\overline{u_x'^2}$, $\overline{u_y'^2}$, $\overline{u_z'^2}$, $\overline{u_x'u_y'}$, $\overline{u_y'u_z'}$, and $\overline{u_z'u_x'}$) and equation for energy dissipation (ε), the total equations are seven partial different transport equations.

The calculation of Reynolds stresses for RSM turbulent model has more complexity than two previous models. All of the six Reynolds stresses terms in RSM model are obtained by using the partial differential form, the exact Reynolds stress transport equations, the detail of these equations can be seen in **Equation (4.1.13)**.

$$
\underbrace{\frac{\partial}{\partial t}\left(\rho\overline{u_i'u_j'}\right)}_{Local\ time\ derivative} + \underbrace{\frac{\partial}{\partial x_k}\left(\rho u_k \overline{u_i'u_j'}\right)}_{C_{ij}=Convection} = \underbrace{-\frac{\partial}{\partial x_k}\left(\rho\overline{u_i'u_j'u_k'} + \overline{p\left(\delta_{kj}u_i' + \delta_{ik}u_j'\right)}\right)}_{D_{T,ij}=Turbulent\ diffusion}
$$

$$
+\underbrace{\frac{\partial}{\partial x_k}\left[\mu\frac{\partial}{\partial x_k}\left(\overline{u_i'u_j'}\right)\right]}_{D_{l,ij}=Molecular\ diffusion} - \underbrace{\rho\left(\overline{u_i'u_j'}\frac{\partial u_j}{\partial x_k} + \overline{u_j'u_k'}\frac{\partial u_i}{\partial x_k}\right)}_{P_{ij}=Stress\ production} - \underbrace{\rho\beta\left(g_i\overline{u_j'\theta} + g_j\overline{u_i'\theta}\right)}_{G_{ij}=Buoyancy\ production}
$$

$$
+\underbrace{\overline{p\left(\frac{\partial u_i'}{\partial x_j} + \frac{\partial u_j'}{\partial x_i}\right)}}_{\phi_{ij}=Pressure\ strain} - \underbrace{2\mu\overline{\frac{\partial u_i'}{\partial x_k}\frac{\partial u_j'}{\partial x_k}}}_{\varepsilon_{ij}=Dissipation} - \underbrace{2\rho\Omega_k\left(\overline{u_j'u_m'}\varepsilon_{ikm} + \overline{u_i'u_m'}\varepsilon_{jkm}\right)}_{Fij=Production\ by\ system\ rotation} + \underbrace{S_\phi}_{soure\ term} \quad (4.1.13)
$$

The terms of C_{ij}, $D_{L,ij}$, P_{ij}, and F_{ij} do not require any modeling. However, the following sections describe the definition of $D_{T,ij}$, G_{ij}, ϕ_{ij}, and ε_{ij} terms.

The turbulent diffusive transport ($D_{T,ij}$) can be modeled as **Equation (4.1.14)**. When the model of turbulent viscosity (μ_t) is similarly computed in standard $k-\varepsilon$ model, which is $\mu_t = \rho C_\mu \dfrac{k^2}{\varepsilon}$ and value of σ_k is 0.82. To denoted that this σ_k value for RSM is slightly difference with the standard $k-\varepsilon$ models, in which $\sigma_k = 1.0$.

$$D_{T,ij} = \frac{\partial}{\partial x_k}\left(\frac{\mu_t}{\sigma_k} \frac{\partial \overline{u'_i u'_j}}{\partial x_k} \right) \tag{4.1.14}$$

The pressure-strain model (ϕ_{ij}) can be written in **Equation (4.1.15)**. Let $\phi_{ij,1}$ is the slow pressure-strain term, $\phi_{ij,2}$ is called the rapid pressure-strain term, and $\phi_{ij,\omega}$ is the wall-reflection term. All of them are modeled as follow.

$$\phi_{ij} = \phi_{ij,1} + \phi_{ij,2} + \phi_{ij,\omega} \tag{4.1.15}$$

$$\phi_{ij,1} = -C_1 \rho \frac{\varepsilon}{k}\left[\overline{u'_i u'_j} - \frac{2}{3}\delta_{ij} k \right] \tag{4.1.16}$$

$$\phi_{ij,2} = -C_2\left[\left(P_{ij} + F_{ij} + G_{ij} - C_{ij} \right) - \frac{2}{3}\delta_{ij}\left(P + G - C \right) \right] \tag{4.1.17}$$

With $C_1 = 1.8$, $C_2 = 0.6$, P_{ij}, F_{ij}, G_{ij}, and C_{ij} are defined in **Equation (4.1.13)**. Moreover, $P = \dfrac{1}{2}P_{kk}$, $G = \dfrac{1}{2}G_{kk}$, and $C = \dfrac{1}{2}C_{kk}$.

The last term in **Equation (4.1.15)**, the wall-reflection term ($\phi_{ij,w}$) is the distribution of normal stresses near the wall. This term is modeled as **Equation (4.1.17)**. Where $C'_1 = 0.5, C'_2 = 0.3$, n_k is unit normal to the wall, d is the normal distance to the wall. And, $C_l = \dfrac{C_\mu^{3/4}}{\kappa}$ while $C_\mu = 0.09$ and $\kappa = 0.4187$.

$$\phi_{ij,w} = C_1' \frac{\varepsilon}{k}\left(\overline{u_k'u_m'}n_kn_m\delta_{ij} - \frac{3}{2}\overline{u_i'u_k'}n_jn_k - \frac{3}{2}\overline{u_j'u_k'}n_in_k \right)\frac{k^{3/2}}{C_l\varepsilon d} \tag{4.1.18}$$

$$+ C_2'\left(\phi_{km,2}n_kn_m\delta_{ij} - \frac{3}{2}\phi_{ik,2}n_jn_k - \frac{3}{2}\phi_{jk,2}n_in_k \right)\frac{k^{3/2}}{C_l\varepsilon d}$$

The buoyancy production term (G_{ij}) is modeled as **Equation (4.1.19)**. When 0.85 is the default of $\Pr_t$ that is the turbulent Prandtl number for energy.

$$G_{ij} = -\frac{\mu_t}{\rho\Pr_t}\left(g_i\frac{\partial\rho}{\partial x_j} + g_j\frac{\partial\rho}{\partial x_i} \right) \tag{4.1.19}$$

Finally, the tensor of dissipation rate (ε_{ij}) is modeled as **Equation (4.1.20)**.

$$\varepsilon_{ij} = \frac{2}{3}\delta_{ij}\left(\rho\varepsilon + 2\rho\varepsilon\frac{k}{a^2} \right) \tag{4.1.20}$$

Where a is the speed of sound. It should be note that the scalar dissipation rate (ε) is computed with a model transport equation similarly to that used in the standard $k-\varepsilon$ model.

4.2 Governing equations for particle motion

FLUENT predicts the trajectory of a discrete phase particle (or droplet or bubble) by integrating the force balance on the particle, which this force balance bases on the Newton's second law. There are many forces that act on a particle in cyclone as centrifugal force, drag force, gravitational force. However, the default of the particle motion equations for FLUENT can be written in **Equation (4.2.1)**.

$$\frac{du_p}{dt} = F_D(u - u_p) + \frac{g_x\left(\rho_p - \rho\right)}{\rho_p} + F_{\phi x}$$
(4.2.1)

Here, u and u_p are the fluid and particle, respectively. $F_{\phi x}$ is the source term. In detail of source term, an additional force can be determined by writing new subroutine into user-define function in FLUENT^{TM}. This user-define function can be defined by writing a computer language to determine the interested effect of new source term; such as electrostatic force, magnetic force etc.

According to the **Equation (4.2.1)**, the definition of F_D is the drag force per unit particle mass, which is shown in detail as **Equation (4.2.2)**. The definition of μ is the molecular viscosity of the fluid, ρ is the fluid density, ρ_p is the density of the particle, and d_p is the particle diameter. Re is the relative Reynolds number.

$$F_D = \frac{18\mu}{\rho_p d_p^2} \frac{C_D \, \text{Re}}{24}$$
(4.2.2)

Equation (4.2.3) shows drag coefficient (C_D) for smooth spherical particles, which a_1, a_2, a_3 are constants that apply over several ranges of Re.

$$C_D = a_1 + \frac{a_2}{\text{Re}} + \frac{a_3}{\text{Re}^2}$$
(4.2.3)

In case of sub-micron particles, when the particle diameter less than 1 micron, the model of drag force will be changed from **Equation (4.2.2)** to **Equation (4.2.4).**

$$F_D = \frac{18\mu}{\rho_p d_p^2 C_C}$$ (4.2.4)

The factor C_C is the Cunningham correction factor to Stokes' drag law. The default of FLUENT is defined in **Equation (4.2.5)**. Here, λ is the molecular mean free path.

$$C_C = 1 + \frac{2\lambda}{d_p}\left(1.257 + 0.4e^{-1.1d_p/2\lambda}\right)$$ (4.2.5)

4.3 Boundary and initial conditions

The boundary conditions for fluid in cyclone are defined in four regions; inlet, upper outlet, blowdown outlet and wall boundary conditions. The details of boundary conditions for two types of cyclone are shown in **Table 4.3.1**.

The Relation of turbulent intensity with k and ε can be shown in **Equation (4.3.1)**. To denoted that D is the characteristic length, $D = \frac{4(area\ of\ inlet\ pipe)}{perimeter\ of\ inlet\ pipe}$.

$$k = 1.5\left(Iu_{inlet}\right)^2 \quad \text{and} \quad \varepsilon = \frac{k^{1.5}}{0.3D}$$ (4.3.1)

From **Table 4.3.1**, it can be seen that the boundary conditions of Reynolds Stress Model (RSM) have the slightly difference from SKE model and $RNG - K - E$ model. The component of Reynolds stresses (R_{ii}, R_{ij}) will be identified at the inlet and outlet of cyclone pipe. **Equation (4.3.2)** indicates all six Reynolds Stress terms.

$$R_{ii} = \overline{u_i' u_i'} = \frac{2}{3}k_{in} \quad \text{and} \quad R_{ij} = \overline{u_i' u_j'} = 0.0$$ (4.3.2)

Table 4.3.1 Summarizing of the boundary conditions

Model	Inlet	Upper outlet	Blowdown outlet	Wall
Cyclone type I				
$k - \varepsilon$	V = 15 m/s I^1 = 10 % and 30 %	P = 0 Pa I^1 = 10 % and 30 %	R^2 = 0 %	Non-slip
$RNG - k - \varepsilon$	V = 15 m/s I^1 = 10 % and 30 %	P = 0 Pa I^1 = 10 % and 30 %	R^2 = 0 %	Non-slip
RSM	V = 15 m/s I^1 = 10 % R_{ii} = 2.25 R_{ij} = 0.0	P = 0 Pa I^1 = 10 % R_{ii} = 2.25 R_{ij} = 0.0	R^2 = 0, 5, 10 and 15%	Non-slip
Cyclone type II				
RSM	V = 10,15,20 and 25 m/s I^1 = 10 % R_{ii} = 2.25 R_{ij} = 0.0	P = 0 Pa I^1 = 10 % R_{ii} = 2.25 R_{ij} = 0.0	R^2 = 0, 5, 10 and 15%	Non-slip

[1] turbulent intensity, [2] ratio of blowdown

4.4 Assumptions

The assumptions of calculation for fluid dynamics can be listed as below:

1. The velocity profile of fluid flow at inlet of cyclones is uniform flow. The injected fluid is also assumed normal with the plane of inlet pipe. It should be noted that the protrusive vortex finder pipe of this investigated system is appropriate length; the dimensionless of the protrusive length to cyclone body is one.

2. The effect of compressibility can be neglected. Although, investigated fluid is compressible air but the compressibility effect is not significant when Mach number less than one.

3. One-way coupling force between particle and fluid is assumed. According to Crowe et. al. (1998) who published the results of investigated that the dilute disperse phase and very fine particle size did not affect to the fluid motion. This system in this research is also dilute and size of particle is 0.1 – 10 micron. Therefore, it is reasonable to assume that this one-way coupling force of particle-air.

4. Time-independent or steady state flow is determined. The investigated cyclone has high flow rate, while volume capacity of cyclone is small. Consequently, the calculation of resident time with the both of cyclones is very short. Therefore, it is necessary to determine the effect of unsteady state condition. However, the effect of unsteady state is the significant factor to calculate the particle trajectory. In short, the unsteady state will be taken into account only the particle motion.

In case of the particle motion, it also has important assumptions.

1. No particle-particle interaction is taken into account in this system because the particle concentration in feed is dilute. For calculating the collection efficiency, only a particle is injected into the cyclone then this process will be repeated for changing inlet position and particle size to calculate the collection efficiency curve.

2. It should be noted that the particle would not rebound with wall when it collide with a wall of dust hopper. Therefore, the fine particle re-entrainment at the lower section of hopper is also not determined.

3. If a particle collides with the interested wall, the calculation will terminate. The interested wall is a region where is defined for particle collection, it can be called trap wall. The detail of this region will describe in next chapter. In contrast, it means that the process of trajectory calculation is still continue if the particle collides with undesired wall, which is called reflect wall.

4.5 Geometry and dimension of cyclones

Table 4.5.1 lists the dimensions of simulated cyclones. There are two types of cyclone to simulate the fluid dynamics and particle motion. The result of experimental by using cyclone type I is published by Yoshida (1996). While cyclone type II, Stairmand's cyclone, is employed for experimental by Dirgo and Leith (1985). It should be noted that the only cyclone type II has protrusive vortex finder.

Table 4.5.1 Dimensions of cyclone separators

	Dimensions			
	Cyclone type I		Cyclone type II	
	[mm]	Dimentionless[1]	[cm]	Dimentionless[1]
Cyclone diameter (D)	40	1.00	30.5	1.0
Cylindrical height (h)	53.2	1.33	45.7	1.5
Cyclone height (H)	162.4	4.06	122.0	4.0
Cone diameter (C)	18	0.45	11.4	0.4
Hopper height (h_H)[2]	100	2.50	76.3	2.5
Hopper diameter (D_H)[2]	42.8	1.07	32.6	1.0
Inlet height (a)	15.2	0.38	15.2	0.5
Inlet width (b)	6.4	0.16	6.1	0.2
Inlet length (I)[2]	40	1.00	30.5	1.0
Outlet height (c)[2]	7.6	0.19	6.1	0.2
Outlet width (d)[2]	6.4	0.16	4.9	0.2
Outlet length (O)[2]	40.0	1.0	30.5	1.0
Blowdown position (B)[2]	15.2	0.38	11.6	0.4
Vortex finder diameter (D_V)	16	0.40	15.2	0.5
Vortex finder protrusive length (V_p)[2]	-	-	15.2	0.5
Vortex finder inserted length (V_I)	63.2	1.58	15.2	0.5

[1] Dimensionless is the relation between the interested length to a cyclone body size.

[2] Additional dimensions
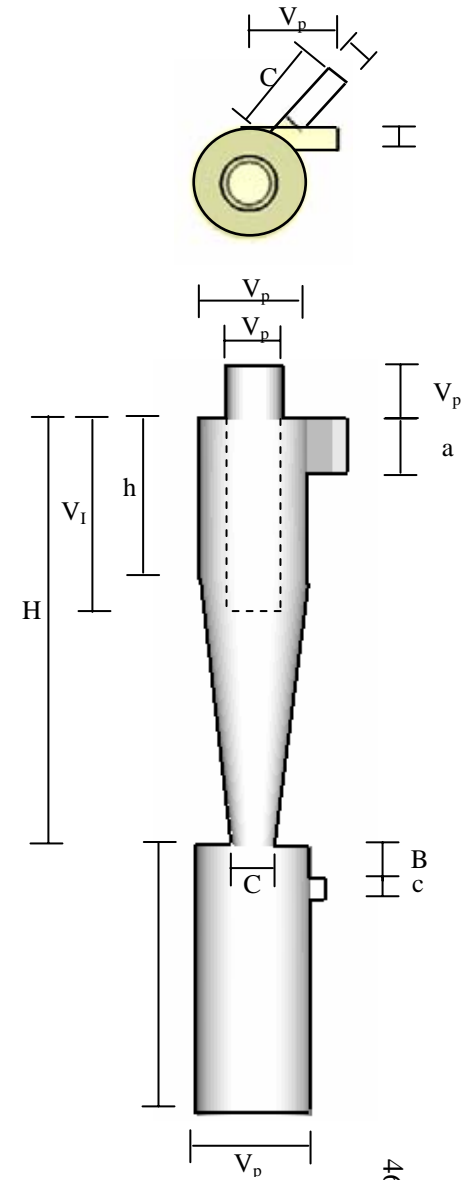
4.6 Simulation conditions of basic case

Table 4.6.1 and **Table 4.6.2** summarize the simulation conditions and model parameter that will be employed for basic case in chapter 5. These simulation conditions and model parameter are obtained from literature reviews and default of commercial FLUENT[TM] program for determining the effect of these conditions on cyclone performance.

Table 4.6.1 Simulation conditions and parameters of fluid phase

Type of cyclone	Type I
Turbulent model	$RNG - k - \varepsilon$ model
Grid size	Coarse size
Turbulent intensity [%]	10%
Protrusive length of vortex finder	-
Residual error	1E-6
Pressure-velocity coupling	SIMPLE
Discretization scheme for convection term	QUICK scheme

Table 4.6.2 Simulation conditions and parameter of particle phase

Length scale (integration time step)	0.1 mm.
Cunningham correction factor in Stoke's law	1.0
Total number of inlet particles	100
Region of particle collection	Hopper
Inlet velocity of particle	Slip condition

CHAPTER V

EFFECT OF SIMULATION CONDITIONS AND MODEL PARAMETER

## 5.1 Effect of simulation conditions and parameter on fluid flow

The three-dimensional conservation equation of mass, momentum and energy are solved by using FLUENT 6.1.22. Beside deviation due to some assumptions, the numerical technique inevitably includes the so-called truncation error and accumulated error. Therefore, the mathematical models and essential parameters should be verified before being employed to simulate the fluid dynamics and particle motion.

5.1.1 Effect of turbulent models

After some tests, the only one turbulent model will be chosen for calculating fluid dynamics within cyclone. There are 3 models, which are standard $k-\varepsilon$ model (SKE), Renormalization Group model ($RNG-k-\varepsilon$), and Reynolds Stress Model (RSM). The derivation of these turbulent models and its assumptions are previously summarized in the criteria to determine the appropriate model. Moreover, some experimentally determined pressure and velocity profile within cyclone is also employed for verification.

In this investigation, first inlet gas velocity is kept constant at 15 m/s in every simulation regardless of the used turbulent models. For the numerical technique, the first or second-order upwind schemes could not be employed, especially for the *RSM* model because their simulating results hardly converged. Therefore, the so-called QUICK (Quadratic Upstream Interpolation for Convective Kinetics) which could provide higher accuracy has been employed instead.

Figure 5.1.1 shows the simulated collection efficiency of cyclone type I, which were predicted by each model. The cut size from experimental result is approximately 1.5 micron. It can be seen that the *RSM* turbulent model can provide the closet collection efficiency. On the other hand, for particles large than the cut size, the $RNG-k-\varepsilon$ model could predict much closer efficiency compared with the experimental result. It should be noted that the simulation results of the *SKE* model much more derivate in all ranges of particle size.
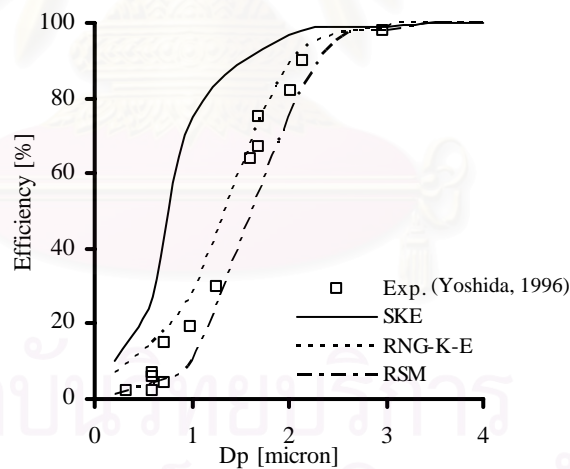
Figure 5.1.1 Effect of turbulent models on collection efficiency

The result of simulation on axial, tangential and radial velocity at three heights of cyclone is shown in **Figures 5.1.2-5.1.4**, respectively. It should be noted that though the axial velocity profile (**Figure 5.1.2**) predicted by the *RSM* model exhibited some deviations compared with the simplest model (*SKE* model), its results was very close to that of the $RNG-k-\varepsilon$ model except at the dust box. Similarly, regarding to the tangential velocity in **Figure 5.1.3**, there are only small derivations among the

prediction results of three models. Moreover, for the radial velocity distribution, because of its low magnitude, there is no significant difference of the predicted results of all models.

Meanwhile, these three models also provided the information of pressure distribution along the considered cyclone as shown in **Figure 5.1.5**. At both upper cylindrical section and middle conical section, the RSM model predicted the highest pressure distribution except at the dust box. On the other hand, if one considers the pressure drop across the cyclone, one will find that the RSM model predicted the lowest value. Integration of the overall pressure drop predicted by all models are compared with the experimental results of Yoshida (1996) in **Table 5.1.1**.

Table 5.1.1 Effect of turbulent models on pressure drop

Model	Pressure drop [Pa]
Experiment (Yoshida,1996)	680
Standard $k - \varepsilon$ model	568
$RNG - k - \varepsilon$ model	532
Reynolds Stress Model	475

The solutions of SKE and $RNG - k - \varepsilon$ turbulent models are significantly difference from RSM model because of derivation of its models [Fredriksson, 1999]. The SKE and $RNG - k - \varepsilon$ turbulent models base on the eddy-viscosity and isotropic assumption. The application of this eddy-viscosity model is reasonable for only simple turbulent flows. In contrast, the Reynolds Stress Model (RSM) solves the partial differential equations for all six Reynolds stress terms. Therefore, the RSM model can represent the complexity of fluid dynamics than the eddy-viscosity model.
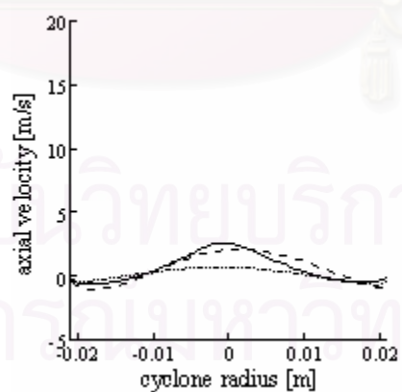
Therefore, when the collection of sub-micron particulate is determined, the appropriate model for predicting fluid flow and particle motion will be the RSM turbulent model. Though, the convergence of this model is strongly difficult and it has under-predicted of pressure drop.
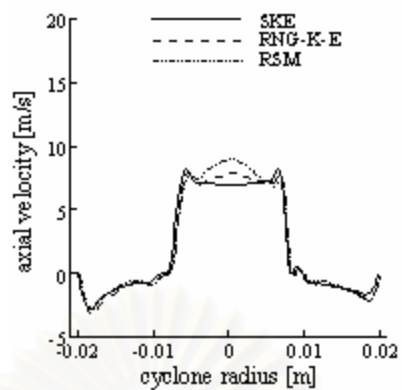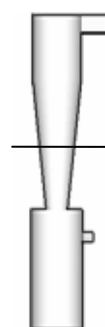
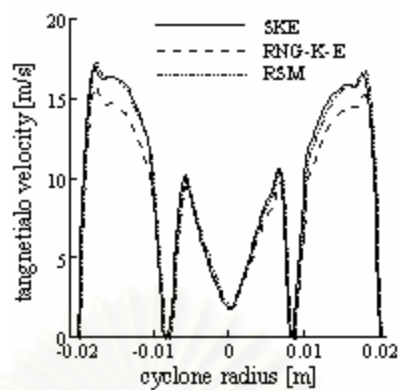a) at the middle of cylindrical section
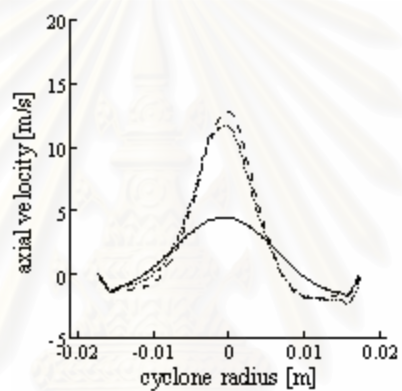
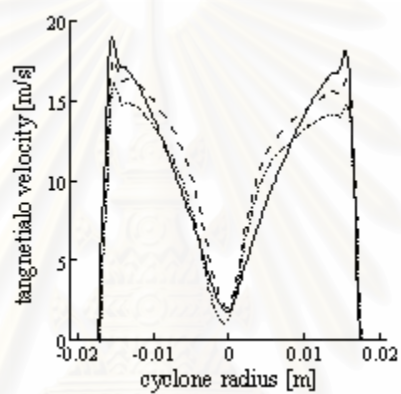

b) at the middle of conical section
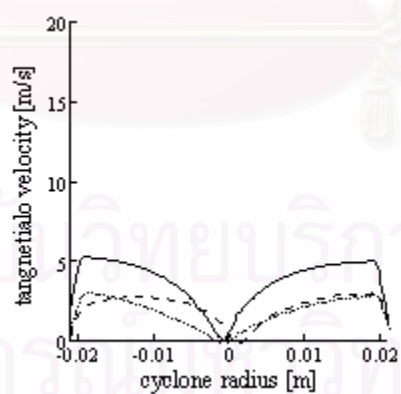

c) at the middle of hopper section

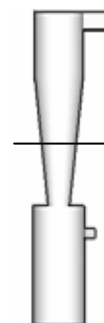**Figure 5.1.2** Effect of turbulent models on axial velocity profiles

a) at the middle of cylindrical section

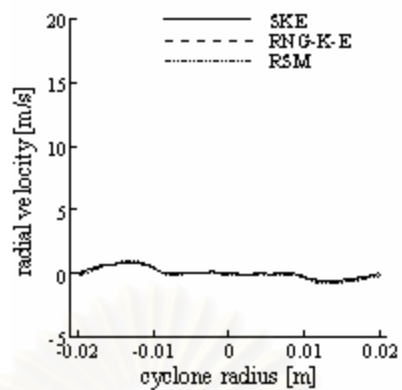b) at the middle of conical section
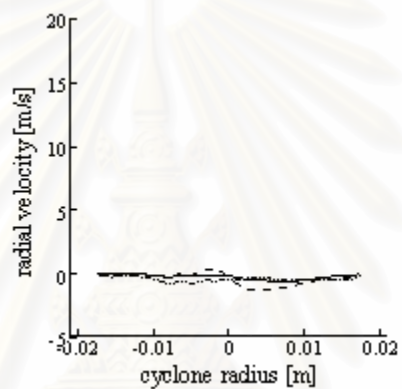

c) at the middle of hopper section

Figure 5.1.3 Effect of turbulent models on tangential velocity profiles

a) at the middle of cylindrical section

b) at the middle of conical section

c) at the middle of hopper section

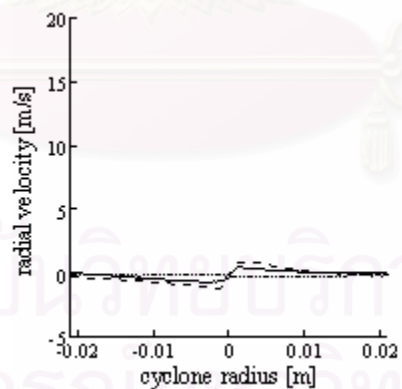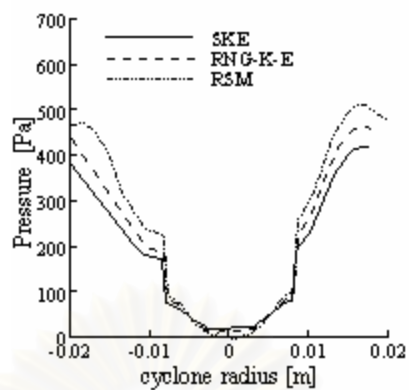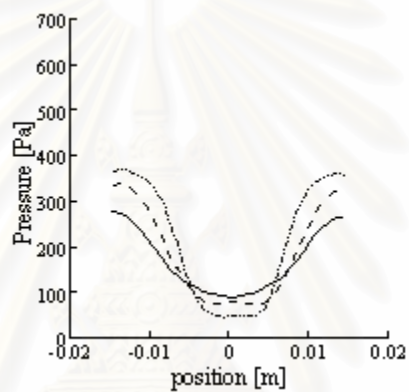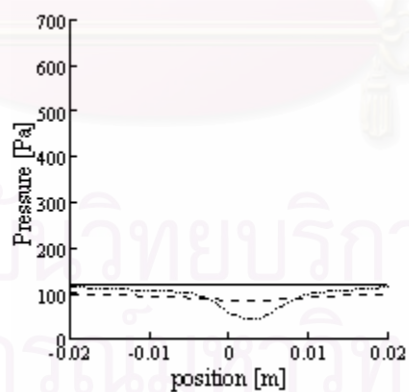**Figure 5.1.4** Effect of turbulent models on radial velocity profiles

a) at the middle of cylindrical section

b) at the middle of conical section

c) at the middle of hopper section

Figure 5.1.5 Effect of turbulent models on pressure profiles

5.1.2 Determination of appropriate grid size

To determine appropriate grid size is one of important processes because some convergence solution is not necessarily a correct one [Chung, 2002]. The geometry of cyclone type I is employed for this matter. The mesh distribution within four regions is unnecessary equal; it depends on velocity gradient. The finer mesh should be generated wherever the high of velocity gradient exist as shown in **Figure 5.1.2** – **Figure 5.1.3**. **Figure 5.1.6** shows that the mesh density is higher at the body of cyclone and conical section due to more rigorous swirl flow in this region. In contrast, the lower mesh density is employed at dust hopper because velocity components are lower in their magnitude. Detail of hexahedral element density in each section is listed in **Table 5.1.2**.

**Table 5.1.2** Amount of elements in each section of cyclone

	Fine grid [Elements]	Coarse grid [Elements]
Inlet pipe	3,375	1,000
Cylindrical section	140,250	32,622
Conical section	70,574	15,934
Dust hopper section	154,474	78,346
Total	368,673	127,902

Figure 5.1.7 illustrates on collection efficiency that is predicted by two different models and two different grid sizes. It can be clearly seen that the result of $RNG - k - \varepsilon$ turbulent model with coarse grid size is close to the experimental result of Yoshida (1996) for larger particles. Meanwhile for smaller particles, finer grid size could provide better prediction when $RNG - k - \varepsilon$ model is employed. For *RSM* turbulent model, the collection efficiency obtained from either coarse and fine grid size is under-predicted when particle size is larger than 1.2 micron.
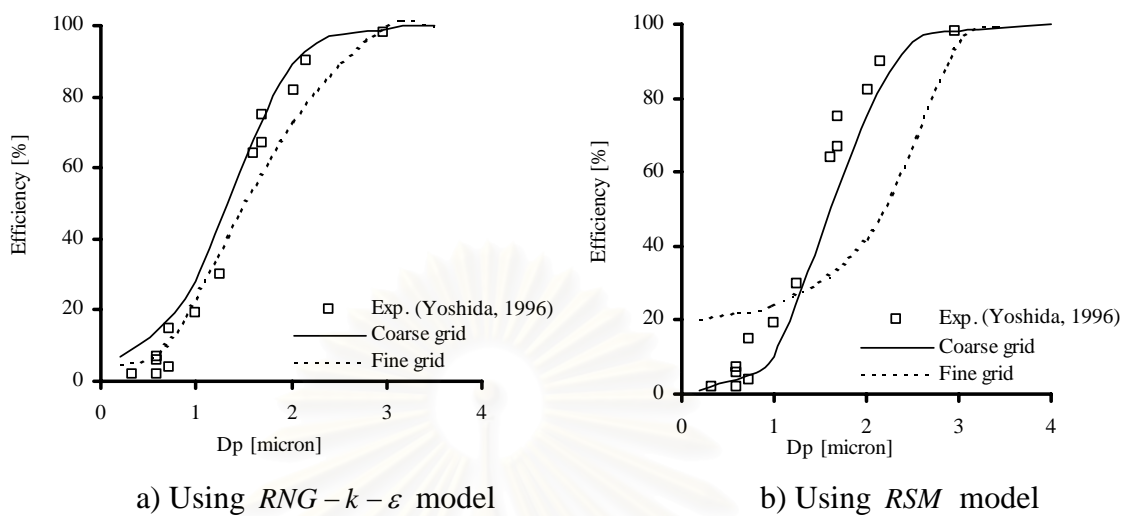
The collection efficiency by using RSM model is lower than the $RNG-k-\varepsilon$ turbulent model. The previous model predicts lower collection efficiency because the simulated tangential velocity is lower than $RNG-k-\varepsilon$ model. Therefore, lower tangential velocity is predicted by using RSM turbulent model resulted in lower collection efficiency compared with that of $RNG-k-\varepsilon$ turbulent model.

Similarly, for the case of $RNG-k-\varepsilon$ turbulent model, grid size exhibits some effects on the predicted tangential velocity. The difference of tangential profile of two grid sizes can be seen in **Figure 5.1.8**. However, the computational required for simulation with finer grid size is much longer time than that of coarse grid size. It should be noted that difference among experimental results and these simulations could be explained as the effect of wall coarseness and the physical disturbance that could not be taken into account in our simulation.

Regarding to the above mention, it could be concluded that coarse grid size defined in **Table 5.1.2** could provide simulation results which is close enough for estimating the actual experimental results of Yoshida (1996) but requires less computational time. Therefore, later simulation will employ this condition to investigate effects of other parameters.

a) Coarse grid size   b) Fine grid size
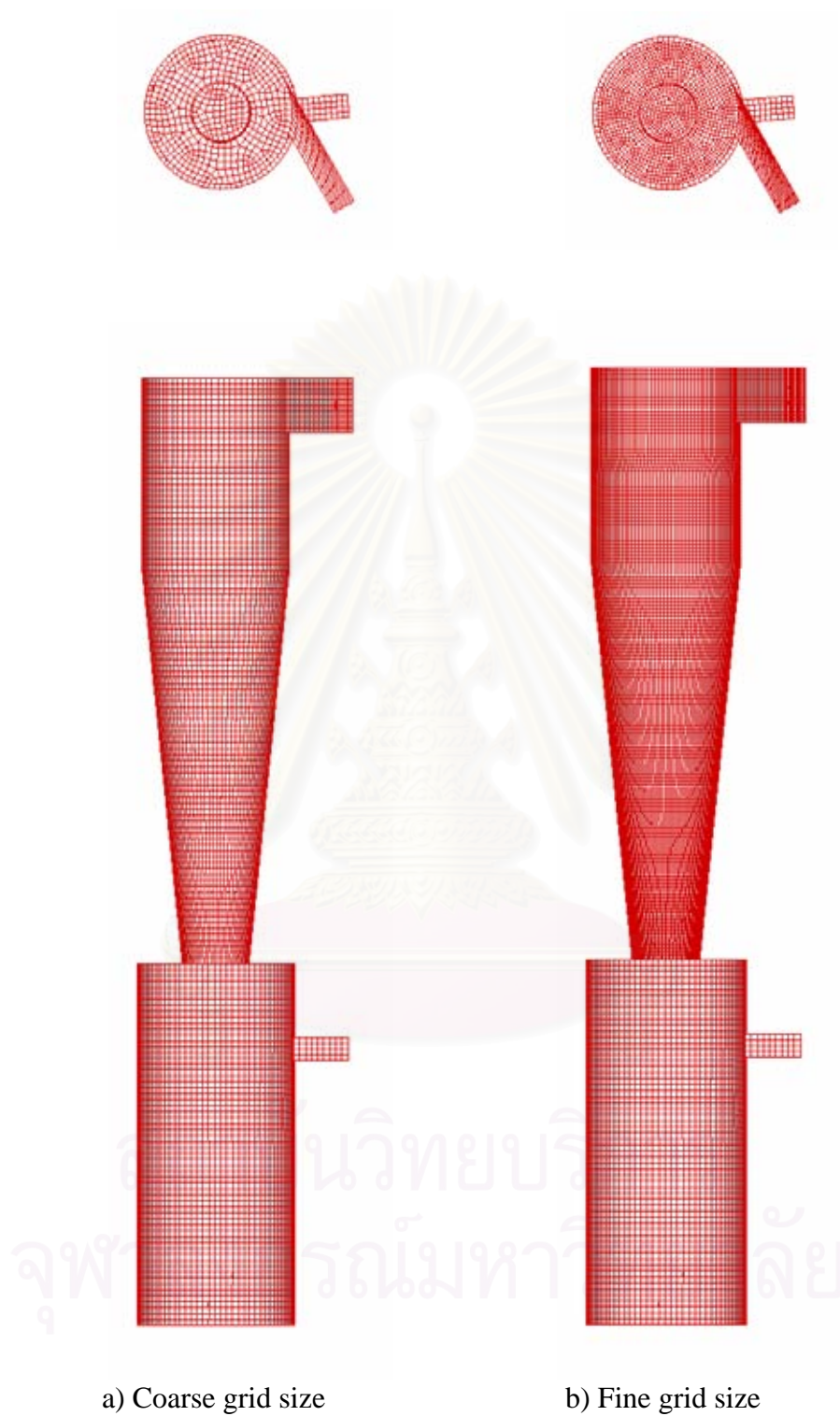
Figure 5.1.6 Grid distribution of cyclone type I

a) Using $RNG - k - \varepsilon$ model   b) Using RSM model

Figure 5.1.7 Effect of grid size on collection efficiency
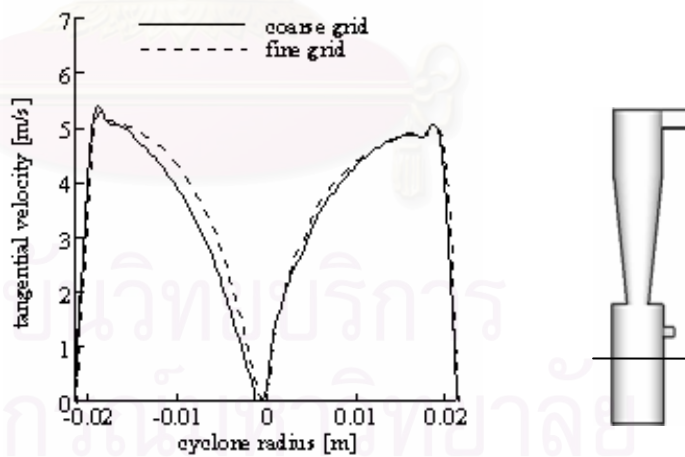
Figure 5.1.8 Comparison of tangential velocity using $RNG - k - \varepsilon$ model

5.1.3 Estimation of appropriate turbulent intensity

Turbulent intensity is an important parameter to be defined at the system boundary condition. In case of inviscid and laminar flow, this parameter is not taken into account. Because in this work, SKE, $RNG-k-\varepsilon$ and RSM turbulent model are employed the appropriate turbulent intensity should be investigated condition.

Turbulent intensity is a ratio of magnitude of turbulent fluctuations to the reference velocity. The criteria for selecting appropriate turbulent intensity are base on the derivation of estimated pressure drop and velocity profiles compared with the referred experimental results and the computational time.

Figure 5.1.9 shows the effect of turbulent intensity on the collection efficiency of the cyclone considered in this work. The result of simulation is compared with experimental result from Yoshida (1996). This figure illustrates turbulent intensity has small effect on the simulated. Simulation results obtained using 10 and 30% are in good agreement with the experimental result. Especially, for particle larger than 1.5 micron, the simulation almost completely coincides with the experiment. When the smaller cut size is determined, the predicted collection efficiency is slightly higher than the experimental because re-entrainment of fine particles is not accountable in the simulation.

It should be noted that with higher turbulent intensity, all terms involving with turbulent effect would become higher, resulting in more difficulty in solving the coupling terms in the conservation equation. Therefore, the computational time consumed in the case of higher turbulent intensity become longer as listed in **Table 5.1.3**. Base on these simulations, turbulent intensity of 10% was selected for investigation.
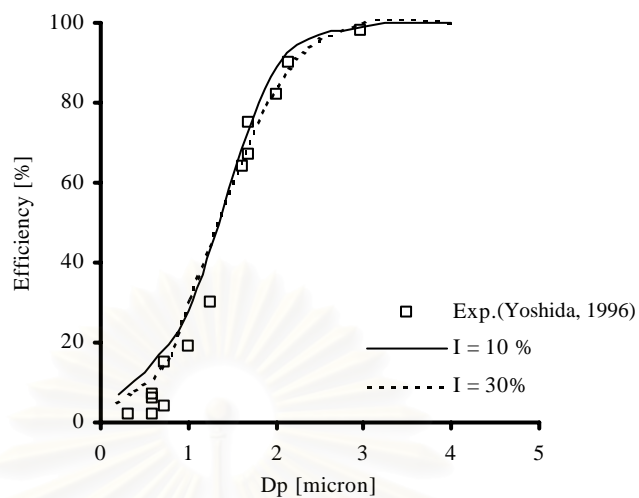
Figure 5.1.9 Effect of turbulent intensity on collection efficiency

Table 5.1.3 Effect of turbulent intensity on pressure drop and computational time

|	Pressure drop [Pa]	Computational time [Hr]
Experimental	680	-
$I = 10\%$	532	14
$I = 30\%$	562	23

5.1.4 Effect of protrusive vortex finder

There are various investigations on cyclone performance which report that the length of inlet and outlet pipe could affect on the cyclone performance [Obermair et. al., 2003; Zhao et. al., 2004; Abrahamson et. al., 2002; Bay et. al., 1997]. Therefore, the effect of protrusive vortex finder should be determined for improving the fluid flow field.

Figure 5.1.10 illustrates the particle trajectory in Cyclone type II, which is employed in the experimental of Dirgo and Leith (1985). The dimensions of protrusive length equal to 0.5 times of cyclone body size.

b) without protrusive pipe   a) with protrusive pipe
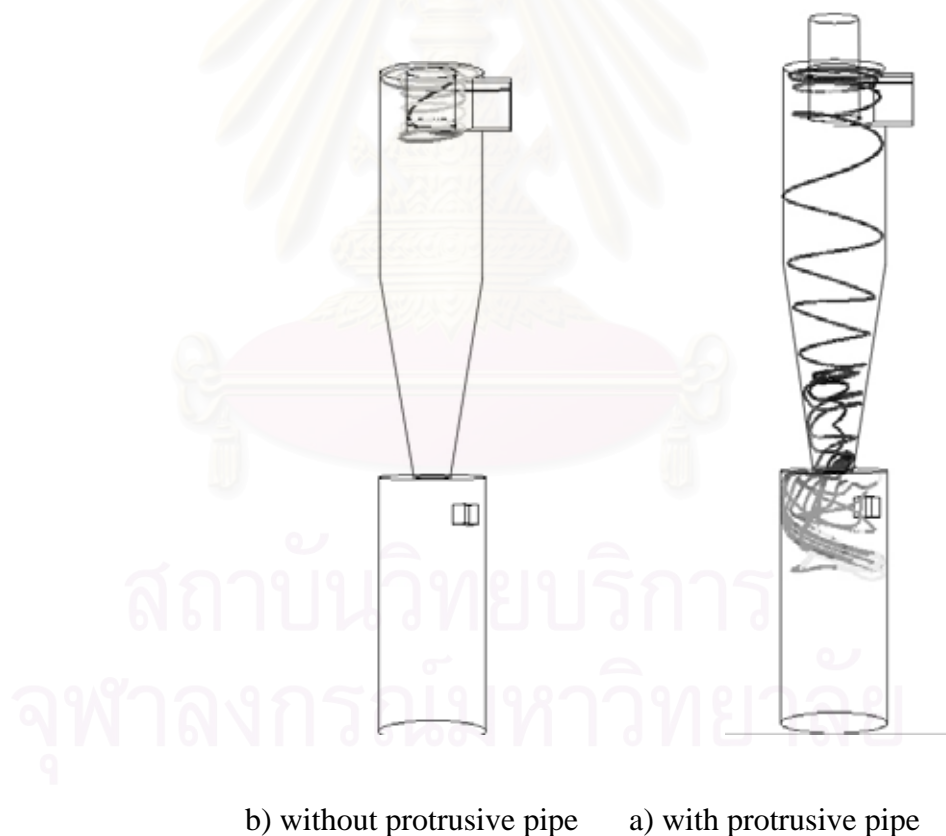
Figure 5.1.10 Effect of protrusive length of vortex finder on particle trajectory

   Figure 5.1.11 shows that the protrusive vortex finder provides some affection on this cyclone collection efficiency. It is clearly seen that the collection efficiency predicted without protrusive pipe is lower than the result with protrusive pipe and experimental data. Especially, D_{50} in the case without protrusive pipe result is clearly lower than the case with protrusive pipe, which could be implied to be in better agreement with the experiment. The simulation result of this cyclone with protrusive pipe can predict collection efficiency well within all range of particle size.
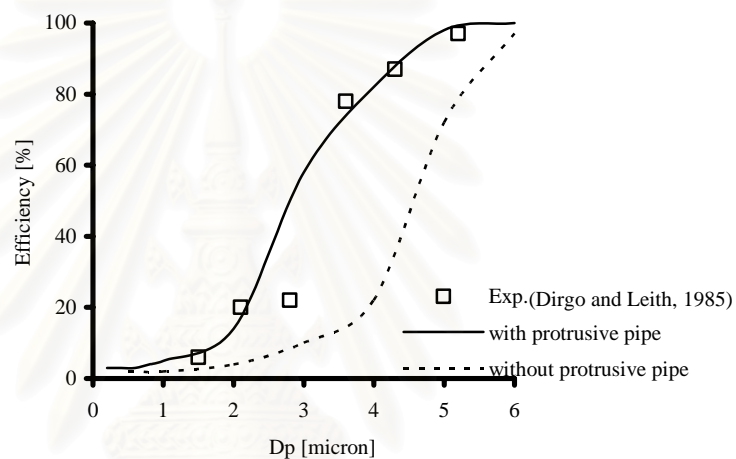
Figure 5.1.11 Effect of protrusive length of vortex finder on collection efficiency

   Figure 5.1.12 shows the simulation results of axial velocity profiles in case with and without protrusive pipe. The simulated result of this cyclone with protrusive pipe indicates that an axial velocity profile at the center core of vortex finder is steeper than the result without protrusive pipe. It can imply that the opportunity of particle collection is higher.
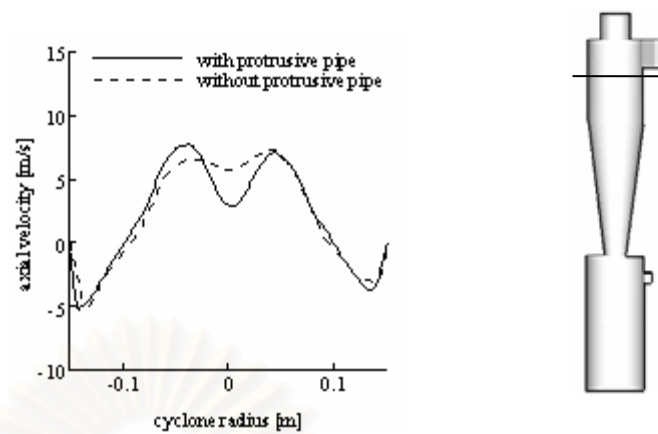
Figure 5.1.12 Effect of protrusive length of vortex finder on axial velocity

Table 5.1.5 lists the pressure drop of these geometries. The difference of simulation results between the case with and without protrusive vortex finder is less than 0.5%. It should be noted that these results are obtained by using *RSM* model that normally gives pressure drop lower than experimental about 22%.

Table 5.1.4 Effect of protrusive vortex finder on pressure drop

	Pressure drop [Pa]
Experimental	785
Simulation result <u>without</u> protrusive pipe	610
Simulation result <u>with</u> protrusive pipe	608

It can be concluded that the cyclone with protrusive vortex finder is necessary to generate for adjusting the collection efficiency of cyclone type II. Regarding to the present simulation, the length for protrusive vortex finder with respect to cyclone body diameter is 0.5, which could provide acceptable results.

5.2 Effect of simulation conditions for particle phase

5.2.1 Determination of length scale (integration time step)

Error of any numerical approximation could be declined by using optimal step size (Blazek, 2001). FLUENT^{TM} program employs the Finite Volume Method (FVM) to convert the partial differential form into the algebraic equations form. Therefore, this error will occur due to approximation of both spatial step size (Δx) and time step size (Δt). Not only grid size but also time step should be optimized to get acceptable results within reasonable computational time.

Length scale (L) is a characteristic value necessary for determination time step for integrating the equations of particle motion. L is equivalent to the distance that a particle will travel before its motion equations and its trajectory are updated. The theoretical integration time step is proportional to length scale as shown in **Equation (5.2.1)**, while u_P and u_F are the velocity of particle and fluid, respectively.

$$\Delta t = \frac{L}{u_p + u_c} \qquad (5.2.1)$$

As shown in **Figure 5.2.1**, the 0.1 mm. length scale could provide the predicted collection efficiency closest to the experimental results of Yoshida (1996). For particle size larger than 1.5 micron, the predictions of any length scales are in agreement with the result of experimental on collection efficiency. However, for particle size smaller than 1.5 micron, the predictions by using the smallest length scale provided the best estimation.

In general, if step size or integration time step becomes smaller, the higher accuracy of prediction of particle motion will be expected [Ferziger and Peric, 1999; Chung, 2002] but the computational time is longer to iterate. The smallest step size usable in our systems is 0.1 mm. because the maximum iteration is limited at 10^9. Therefore, this 0.1 mm. value of length scale will be employed for predicting a particle motion within two types of cyclone.
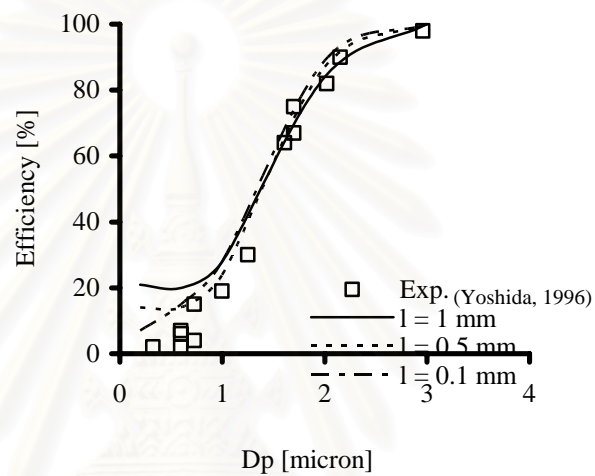

Figure 5.2.1 Effect of length scale on collection efficiency

5.2.2 Effect of Cunningham correction factor

The Cunningham correction factor is employed to adjust the result of drag force for sub-micron particulate as shown in **Equation (4.2.4)**.

In this section, the effect of Cunningham correction factor on cyclone collection efficiency is studied. **Figure 5.2.2** illustrates the effect of Cunningham correction factor in the cyclone investigation by Yoshida (1996). The result indicates that Cunningham correction factor provides higher collection efficiency. Especially, when particle size is smaller than 0.5 micron, deviation between the results of simulation and experimental becomes larger. This higher deviation implied as enhancement of fine particle collection due to diffusion mechanism. Those fine particles will come to contact with and then deposit on the wall. However, in the actual condition, those particles do not totally deposit on but rebound back into the core region (low pressure region) before swirling up to escape from cyclone separator. For larger particles, Cunningham correction factor has no significant effect on particle motion as well as their collection efficiency.
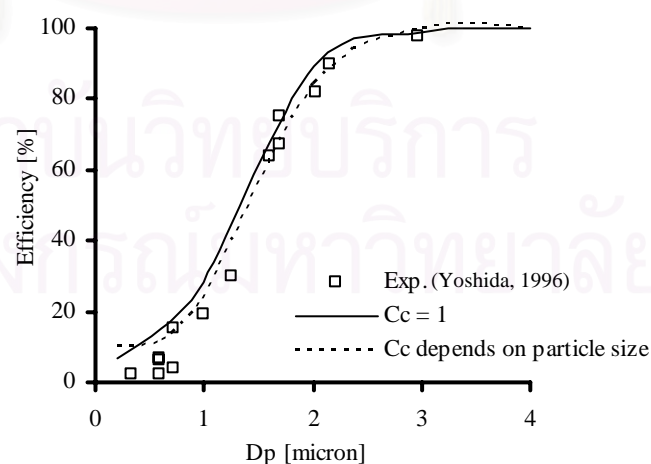
Figure 5.2.2 Effect of Cunningham correction factor

5.2.3 Effect of the sampling amount of inlet particle

Figure 5.2.3 shows the effect of total number of inlet particles. It is clearly seen that when the sampling amount of each particle is varied between 100 and 1,000 particle, the simulated collection efficiency significantly larger than experimental of Yoshida (1996). Interesting to with the higher total amount of inlet particle, wider difference between experimental and simulation could be observed especially in the range of particles smaller than 1.8 micron. This could be implied that in case of higher the amount of inlet particle the possibility of particle traveling close to the wall of cyclone is also higher. Therefore, in this work 100 particles is selected as the suitable total number of inlet particle.
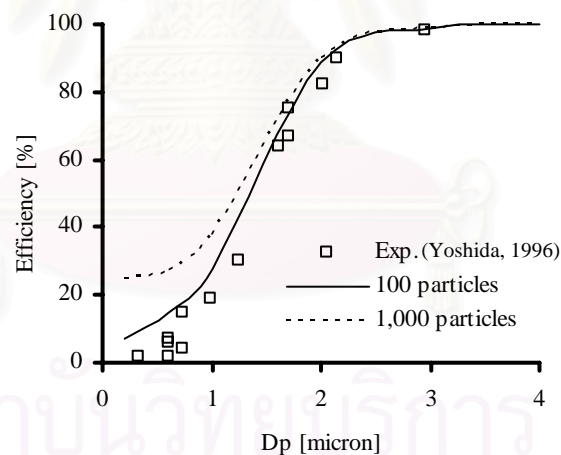

Figure 5.2.3 Effect of the total number of inlet particle

### 5.2.4 Effect of region of particle collection

It is reasonable to assume that there are three regions for particle collection. The first region is the whole area of conical and hopper section. The second region is combined area of half of conical section and the hopper section. The third region for particle collection is the wall of dust hopper. When a single particle collides with this interested region, this particle will be assumed to collecte in cyclone separator.

Figure 5.2.4 illustrates the effect of these assumed regions for particle collection with wall of cyclone. It can be observed that the deviation of simulated results from region 2 and 3 is higher than that of region 1. The simulated results with assumption of region 2 and 3 are over-predicted on 0.2 – 2 micron. For instance, the collection efficiency of region 2 and 3 at 1.5 micron is much deviation from the experimental of Yoshida (1996). The deviation of collection efficiency at 1.5 micron between experimental and simulation of region 1, 2 and 3 are 2%, 23% and 32%, respectively. However, for particle whose size is larger than 2 micron, deviation of experimental and simulation become smaller because fine particle can re-entrain from hopper.

Figure 5.2.5 illustrates the typical of particle trajectory in cyclone type I. It could be simply explained that the particle could be more collected when larger collection area is assumed. The particle can escape from cyclone in case of region 1 while particle is collected by wall of conical section if the collected wall is region 2.
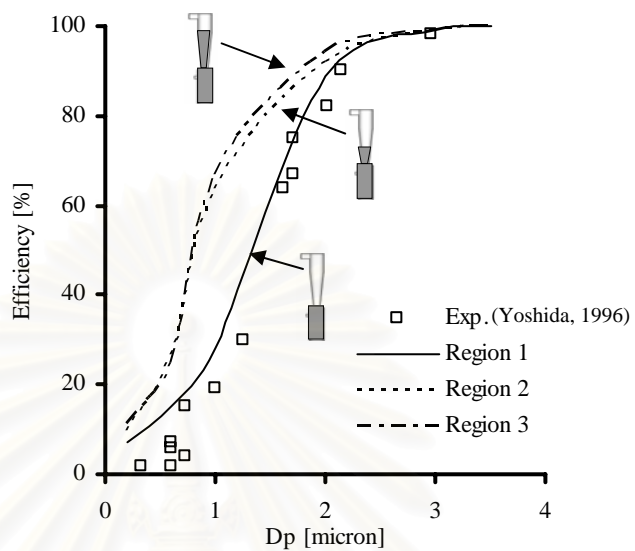
Figure 5.2.4 Effect of region of particle collection
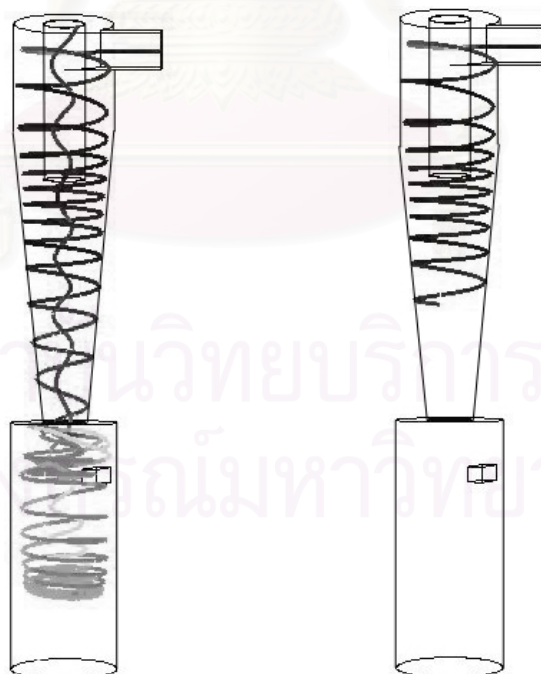
a) Region 1   b) Region 2

Figure 5.2.5 Effect of collected region on particle trajectory

CHAPTER VI

RESULTS AND DISCUSSIONS

6.1 Adopted simulation conditions

In chapter 5, many simulation conditions and model parameters are investigated for verification of their appropriate values. These appropriate simulation conditions are employed to predict the fluid dynamics and particle trajectory within two types of cyclone. In this chapter, the collection efficiency and the pressure drop across the cyclones are calculated. Other additional conditions of simulation such as the residual error, the method of pressure-velocity coupling and discretization scheme for convection terms will be also defined. The details of verified parameters listed in **Table 6.1.1** and **6.1.2**. These tables contain adopted conditions of simulation for fluid and particle phase.

Table 6.1.1 Adopted simulation conditions for fluid phase

Turbulent model	*RSM* model
Grid size	Coarse size
Turbulent intensity [%]	10%
Protrusive length of vortex finder	$0.5 \times D_{cyclone}$
Residual error	1E-6
Pressure-velocity coupling	SIMPLE
Discretization scheme for convection terms	QUICK

Table 6.1.2 Adopted conditions of simulation for particle phase

Length scale (integration time step)	0.1 mm.
Cunningham correction factor in Stoke's law	1.0
Total number of inlet particles	100
Region of particle collection	Hopper

6.2 Relevant experimental results

Experimental results of Yoshida (1996), and Dirgo and Leith (1985) are selected to verify the mathematical models.

The first reference is the experimental of collection efficiency by Yoshida (1996). In **Figure 6.2.1**, the x-axis is the square root of dimensionless inertial parameter ($\sqrt{\psi}$), while y-axis is the collection efficiency [%]. The collection efficiency with 10% blowdown and without blowdown is compared with the simulation result by using $k-\varepsilon$ model in **Figure 6.2.1**. The test particle is monodisperse latex particle ($D_p = 0.33$ - 2.95 micron) with density of 1150 kg/m^3. The characteristic dimensions of this cyclone are listed in **Table 4.3.1**. The body size of air cyclone is 4 cm. The flow rate of particle and air are 2 g/min and 0.148 m^3/min, respectively.
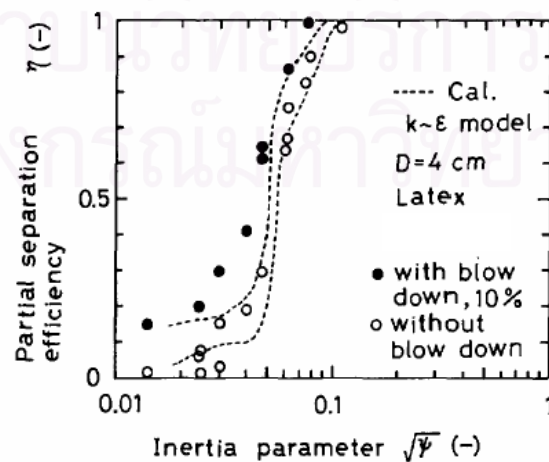
Figure 6.2.1 Experimental result of collection efficiency by Yoshida (1996)

As second reference, Dirgo and Leith (1985) investigated on cyclone performance of Stairmand's cyclone of which cyclone diameter is 30 cm. It should be noted that this cyclone is 7.5 times larger than the previous one. The notation dimensions of this cyclone are also listed in **Table 4.3.1**. The properties of air are ρ_{air} = 1.29 kg/m^3 and η_{air} = 1.75 x 10^{-5} Pa.s, while particle density is 1550 kg/m^3.

Table 6.2.1 lists the experimental result of pressure drop of Dirgo and Leith (1985). The inlet velocities of fluid are varied from 10 to 25 m/s. It should be noted that Dirgo and Leith also investigated the inlet velocity of fluid at 5 m/s but this velocity is not taken into account in this research because the collection efficiency to collect the sub-micron particle is low. The collection efficiency of particle with nominal size of 3.8 micron is only 2%.

Table 6.2.1 Experiment result of pressure drop by Dirgo and Leith (1985)

Inlet [m/s]	Pressure drop [Pa]
10	337
15	785
20	1,407
25	2,205

Figure 6.2.2 also shows the experimental results of collection efficiency investigated by Dirgo and Leith (1985). It can be seen that the minimum and maximum of collected particle size is about 1.5 and 6 micron, respectively. Moreover, the collection efficiency curve becomes sharper, when the inlet velocity is increased. Therefore, installation of blowdown pipe to withdraw fluid from hopper section could result in a decrease in collected particles size.

a) Inlet 10 m/s

b) Inlet 15 m/s

c) Inlet 20 m/s

d) Inlet 25 m/s
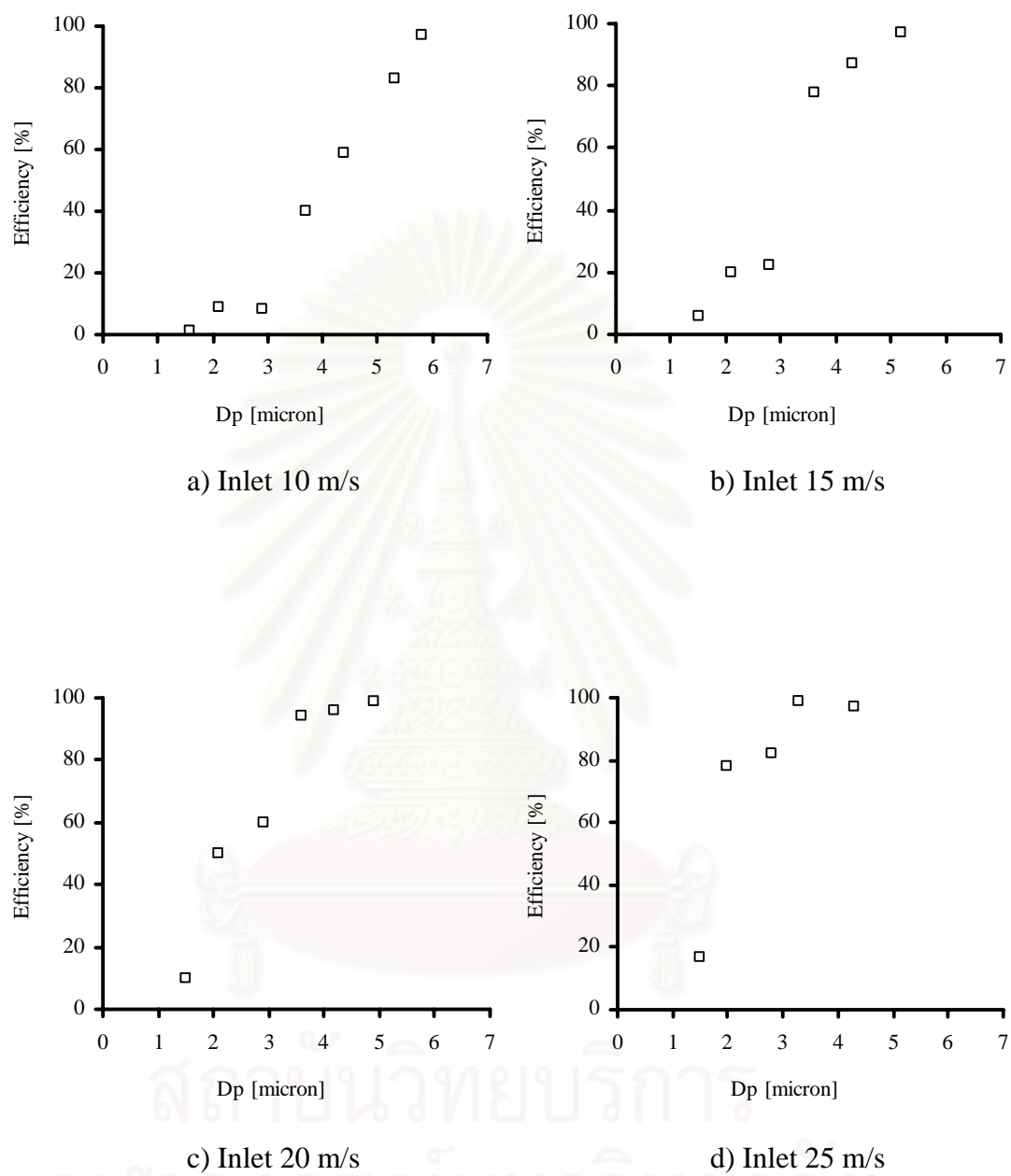
Figure 6.2.2 Experiment result of collection efficiency by Dirgo and Leith (1985)

6.3 Effect of operating variables on cyclone type I

6.3.1 Effect of particle inlet positions

The effect of particle inlet positions on the opportunity of particle collection in cyclone type I is studied in this section. To investigate this effect can be done by observing the particle trajectory that is injected into the inlet plane.

Figure 6.3.1 illustrates the cross sectional area of inlet pipe of cyclone type I. This area is divided into four regions. The position of region I, II, III and IV are close to inner wall at the top, outer wall at the top, inner wall at the bottom, and outer wall at the top, respectively.
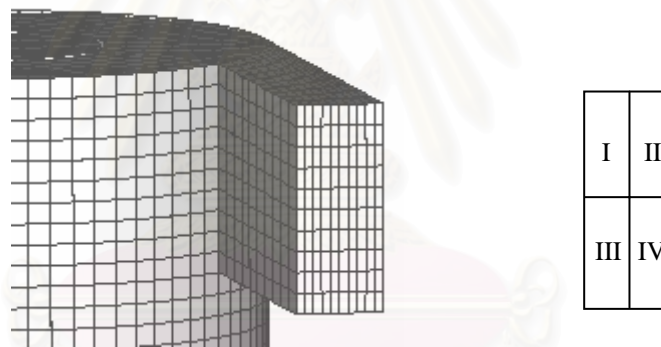
Figure 6.3.1 Four regions of inlet plane

Figure 6.3.2 illustrates the trajectory of particle with 0.5 micron. This particle is injected into each region for investigating the trajectory of particle. It can be observed that the opportunity of particle collection is larger when a particle is injected into the region IV. The trajectory of this particle is swirling down into the hopper then it escapes from this cyclone.

Moreover, it can be seen that the trajectory of particle in **Figure 6.3.2 a)** and **b)** is almost similar. A particle slips down on the wall of vortex finder before it swirls up into vortex finder tube. This fine particle cannot collide with wall of cyclone because it has lower centrifugal force.

Figure 6.3.3 illustrates the trajectory of larger size of particle. A particle with 1.5 micron is injected into four regions for comparing its trajectory. Opportunity of particle collection increases when particle with 1.5 micron is injected into region III. This particle collides with wall of cyclone and swirls down into hopper section. It can be observed that a particle is injected in region I and II still escape from this cyclone because this particle trajectory locates in force vortex. The direction of force vortex is upward direction.
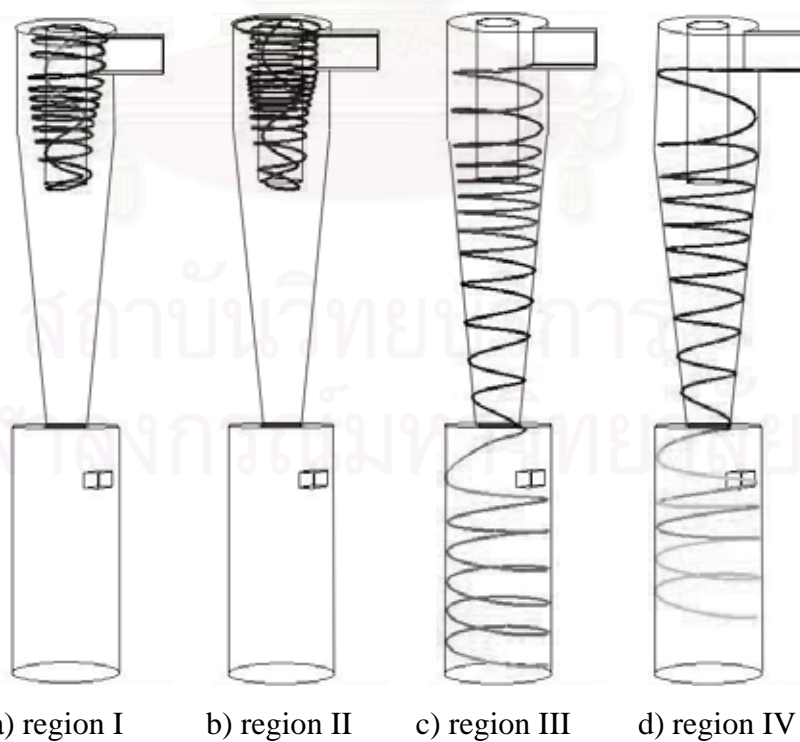
Figure 6.3.4 illustrates that the trajectory of particle with 3 micron. It clearly seen that the opportunity of particle collection is equal. Particle with 3 micron that is injected into the Region I, II, III and region IV can be collected. Moreover, it can be observed that the particle trajectory in **Figure 6.3.4 a)** and **Figure 6.3.4 b)** is similar. There are many circular motion of particle in upper section before swirls down into hopper. **Figure 6.3.4 c)** and **Figure 6.3.4 d)** has also trajectory of particle.

Figure 6.3.5 illustrates the trajectory of particle with 0.5 micron and 3 micron. This particle is injected into the region that locates closes to outer wall at the top region (region II). From the results of simulation, the smaller particle swirls down to the conical section then escapes from the cyclone. This smaller particle cannot collide with wall due to lower centrifugal force. The larger particle collides with cyclone wall because it has higher centrifugal force. This larger particle swirls down in the semi-free vortex so the opportunity of particle collection is higher.
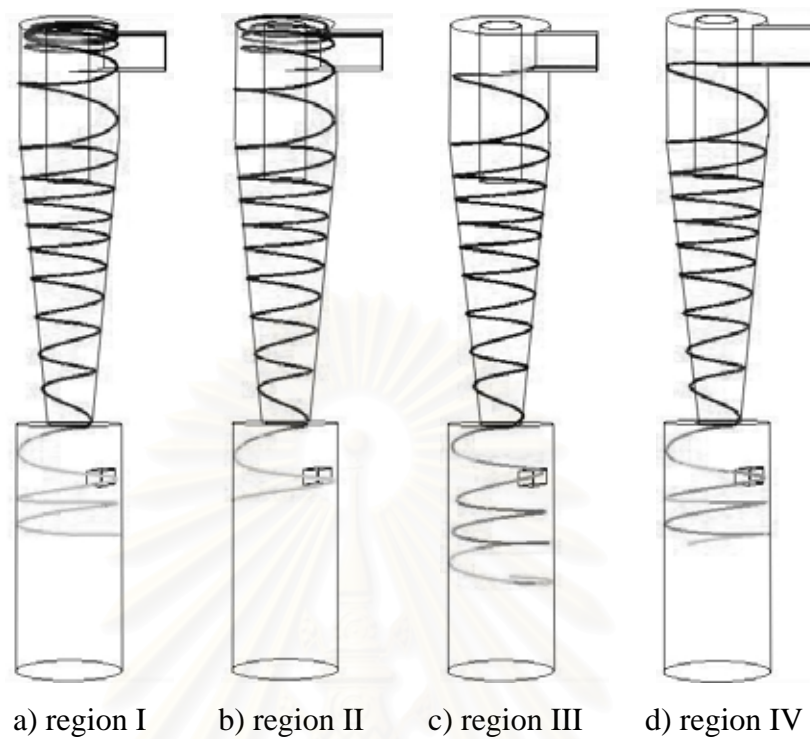
In short, region that closes to the outer wall at the bottom (region IV) is the highest effective zone. This region has the higher opportunity of particle collection than other one because the particle swirls down into semi-free vortex. The semi-force vortex has downward direction. Therefore, the possibility of particle collection will increase. To order the lower effective regions are region III (lower-left), II (upper-right) and I (upper-left), respectively.
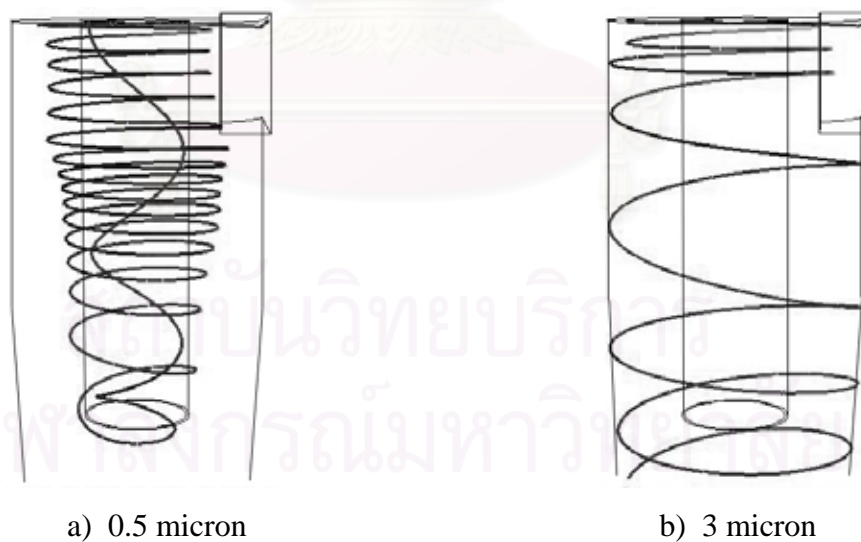
a) region I   b) region II   c) region III   d) region IV
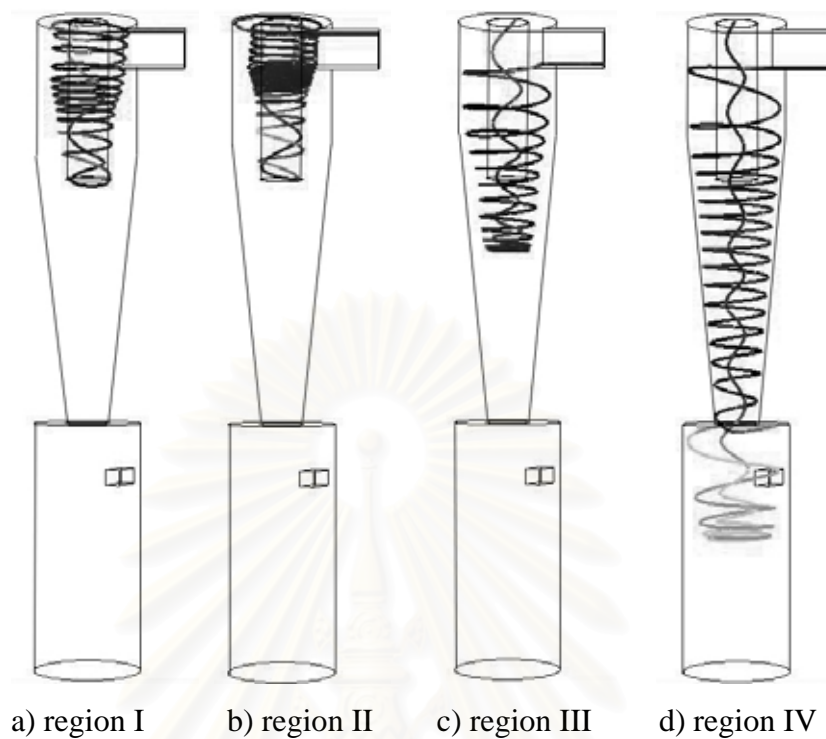
Figure 6.3.2 Trajectory of particle with 0.5 micron in cyclone type I

a) region I   b) region II   c) region III   d) region IV

Figure 6.3.3 Trajectory of particle with 1.5 micron in cyclone type I

a) region I b) region II c) region III d) region IV

Figure 6.3.4 Trajectory of particle with 3 micron in cyclone type I

a) 0.5 micron b) 3 micron

Figure 6.3.5 Trajectory of particle injecting to the outer wall at the top region

6.3.2 Effect of blowdown ratio

Figure 6.3.6 illustrates comparison of experimental result of Yoshida (1996) and simulated result by using *RSM* turbulent model. It can be found that the result of simulation is in good agreement with experimental data. This figure shows that the blowdown ratio affects to collection efficiency of cyclone type I. The collection efficiency is higher when the ratio of blowdown increases to 10%. Especially, particle with 0.3 micron is more collected from 2% to 15%. In addition, the cut size is decreased from about 1.6 micron to 1.2 micron.

Figure 6.3.7 illustrates the effect of ratio of blowdown on collection efficiency by using the numerical technique. The *RSM* turbulent model is employed to predict the collection efficiency of cyclone with and without blowdown. It can be observed that using aspiring air from the top part of hopper section collects the sub-micron particle. For sub-micron particle, the collection efficiency can be increased from 2% to 28% when the blowdown ratio increases to 15%. Moreover, using blowdown decreases the cut size from 1.6 micron to 0.8 micron.

Table 6.3.1 lists the simulated pressure drop across the cyclone type I. The simulated pressure drop is increased from 475 Pa to 583 Pa (pressure drop is increased 26%) when the ratio of blowdown increases from 0% to 15%.

Figure 6.3.8 illustrates the contour of axial velocity within cyclone type I with and without blowdown. The result of simulation shows that the axial velocity at the lower part of conical section has the higher downward direction when the ratio of blowdown is increased. Therefore, the possibility of particle move into the hopper section to collect is higher. Moreover, the non-symmetry flow is easily observed when the ratio of blowdown is increased due to the complexity of fluid flow field in hopper.

Figure 6.3.9 illustrates the effect of blowdown ratio on tangential velocity within cyclone type I. It can be seen that the tangential velocity near the wall of conical section slightly changes when the ratio of blowdown increases. In dust hopper section, it can be observed that the magnitude of tangential velocity increases due to effect of aspired fluid.

Figure 6.3.10 illustrates the contour of pressure in cyclone type I. It can be seen that the core region along this cyclone has lower pressure than the region closet to wall. When ratio of blowdown increases from 0% to 15%, the pressure at core region in hopper section will decrease from about 100 Pa to -20 Pa. Therefore, the fine particle could move into this low pressure zone before entrain from cyclone.

Figure 6.3.11 illustrates the trajectory of particle of 1 micron. This particle is injected into cyclone type I with the inlet air velocity of 15 m/s. In case without blowdown, this particle escapes from the cyclone by traveling into conical section before its trajectory is swirling up into vortex finder tube. In case with blowdown, the possibility of particle collection by colliding with the wall of hopper is higher.

In short, the ratio of blowdown affects to the collection efficiency due to the higher opportunity of particle traveling into dust hopper section. In addition, the pressure drop is slightly increased, as the ratio of blowdown is higher. Therefore, the aspired air from hopper is the good method for collecting or separating the sub-micron particle from carry fluid.
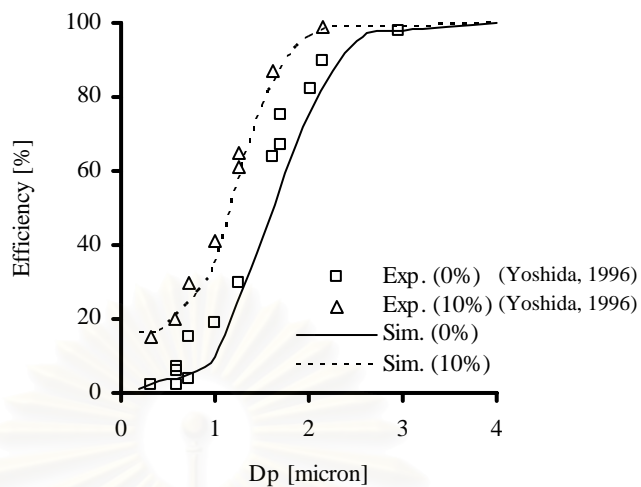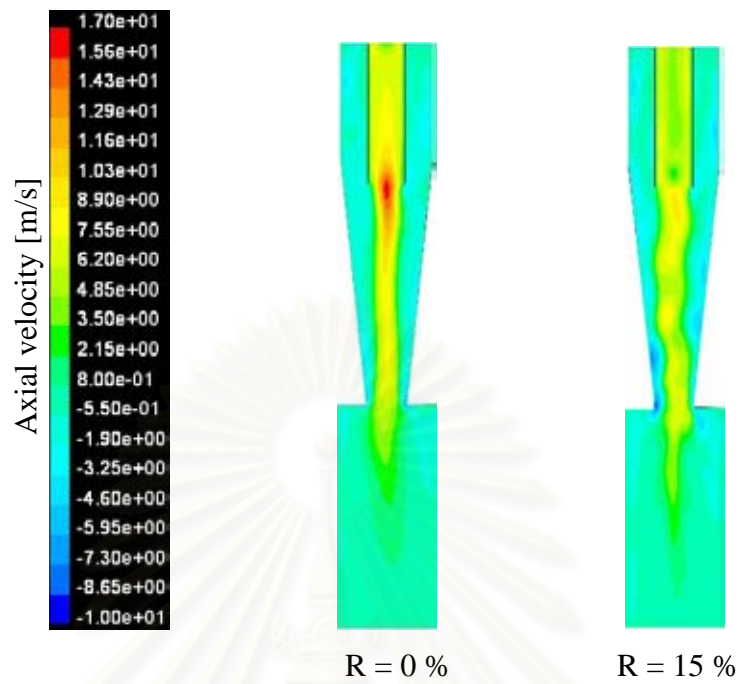
Figure 6.3.6 Comparison of experimental data from Yoshida (1996) and
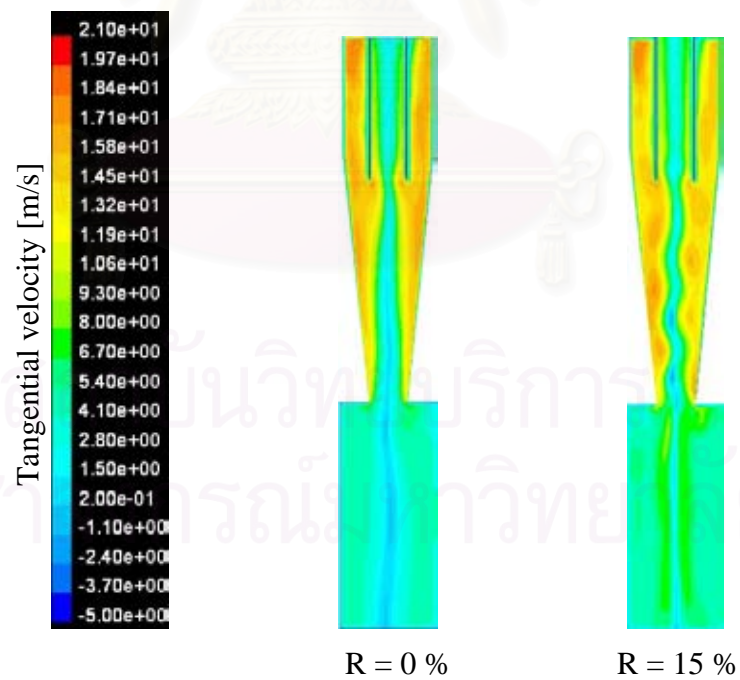simulated results on collection efficiency
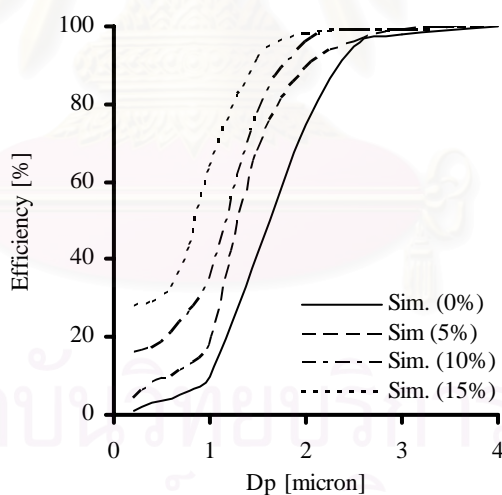
Figure 6.3.7 Effect of blowdown ratio on collection efficiency

Table 6.3.1 Effect of blowdown ratio on simulated pressure drop

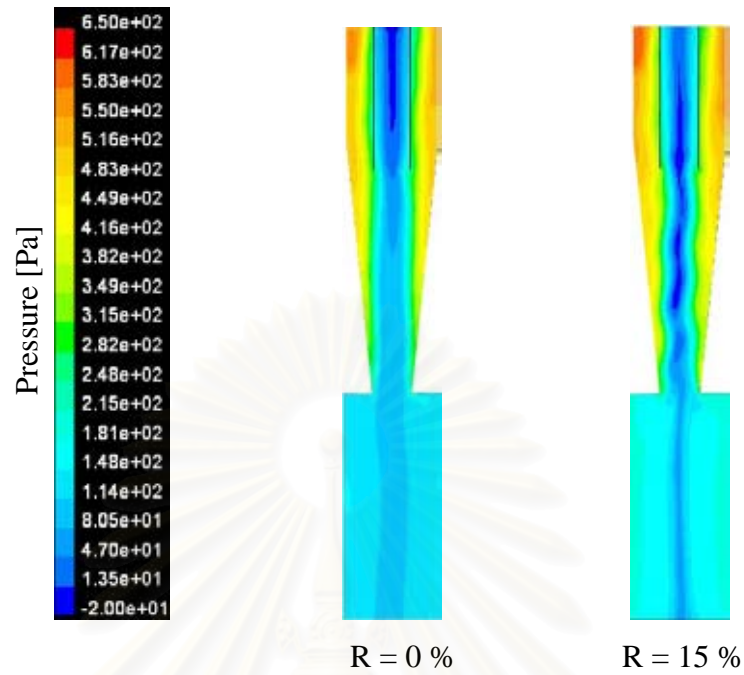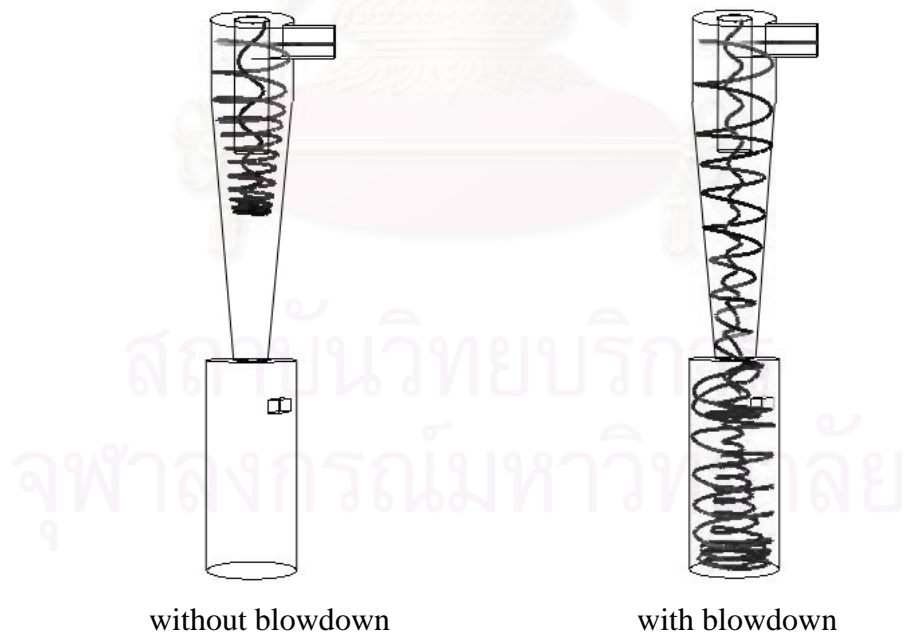| Ratio of blowdown [%]	0	5	10	15
Pressure drop [Pa]	475	516	547	583

Figure 6.3.8 Effect of the ratio of blowdown on axial velocity

Figure 6.3.9 Effect of the ratio of blowdown on tangential velocity

Figure 6.3.10 Effect of the ratio of blowdown on pressure distribution

Figure 6.3.11 Effect of the ratio of blowdown on particle trajectory

6.4 Effect of operating variables on cyclone type II

6.4.1 Effect of inlet air velocity

Figure 6.4.1 shows the results of experimental by Dirgo and Leith (1985) and numerical of pressure drop across cyclone type II. The relation between pressure drop and inlet air velocity could be obtained by using logarithm axis. Pressure drop can be written in the function of inlet air velocity as shown below.

Exp. of Dirgo and Leith (1985)   ; $\Delta P = 3.018V^{2.050}$ (6.4.1)

Simulation   ; $\Delta P = 3.143V^{1.995}$ (6.4.2)

Shepherd and Lapple model   ; $\Delta P = 4.141V^{2.000}$ (6.4.3)

Coker model   ; $\Delta P = 2.451V^{2.000}$ (6.4.4)

The simulation by using *RSM* turbulent model provides slightly deviation between experimental and simulation. This deviation of coefficient is only 4%, while the deviation of power value is 2%. Therefore, it can be seen that our simulation result is better agreement with experimental data than these two models.

Figure 6.4.2 shows the effect of inlet air velocity on the collection efficiency of cyclone type II. It can be observed that the cut size (D_{50}) decreases as the inlet air velocity is increased. This cut size will be decreased to 4.2, 3.0 micron, 2.2 micron, and 1.6 micron when inlet air velocity is increased to 10 m/s, 15 m/s, 20 m/s and 25 m/s, respectively. These figures also show that the collection efficiency curve is sharper for higher inlet air velocity. Therefore, the fine particle could be more collected when inlet air velocity increases.

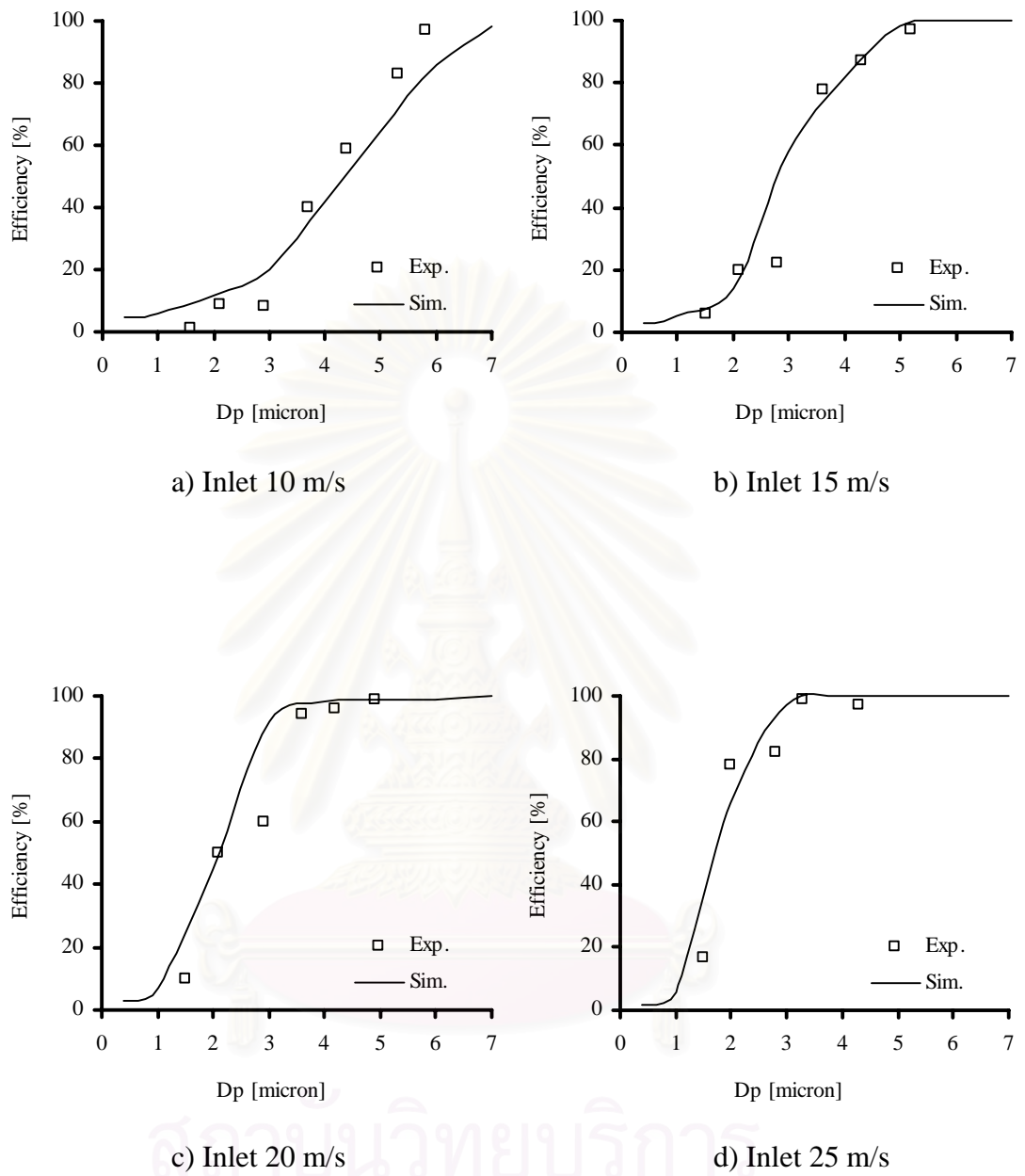**Figure 6.4.3** shows the contour of tangential velocity of air cyclone type II. The blue and red color represents the lowest and highest magnitudes of tangential velocity. It can be seen that the magnitude of tangential velocity in cylindrical and conical section is higher when the inlet air velocity is increased. This increasing tangential velocity will increase the opportunity of particle collision with cyclone wall.

Figure 6.4.4 shows the effect of inlet velocity on pressure in cyclone type II. It can be observed that the pressure at core region becomes lower when the inlet air velocity is increased. In other region, the pressure near wall in the cylindrical and conical becomes higher as the inlet air velocity is increased. It can be mention that the sub-micron particle will easily entrain to escapes from cyclone. In practical, apex cone is employed to avoid this re-entrainment of fine particle [Obermair et. al. (2003); Yoshida et. al. (2001)]

In short, the increasing inlet air velocity provides the smaller cut size and the higher collection efficiency. However, the pressure drop is significantly increased by proportional to the square of inlet air velocity. Additional, the opportunity of re-entrainment of sub-micron particle becomes higher when the inlet air velocity is increased. Therefore, the improvement of cyclone to collect the sub-micron particle by increasing inlet air velocity has the limitation.
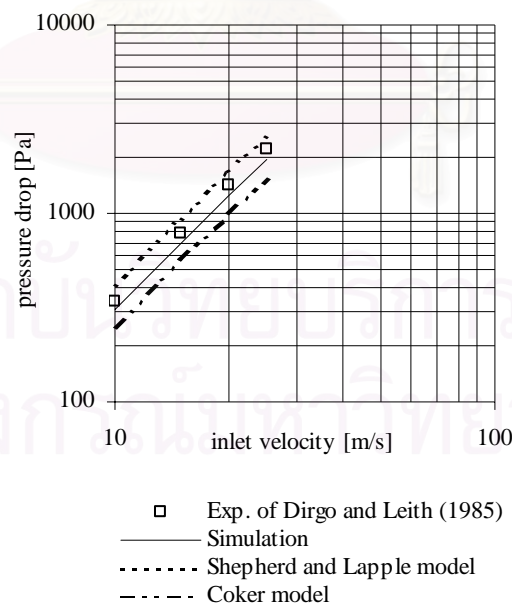
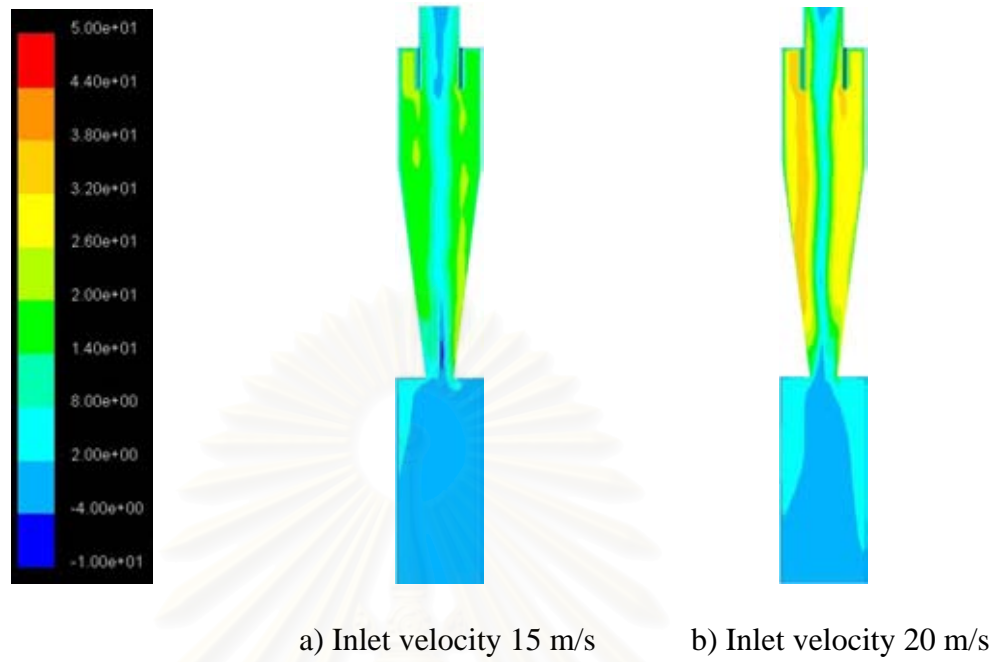**Figure 6.4.1** The pressure drop across cyclone type II for fluid velocity of 10-25 m/s

a) Inlet 10 m/s

b) Inlet 15 m/s

c) Inlet 20 m/s

d) Inlet 25 m/s
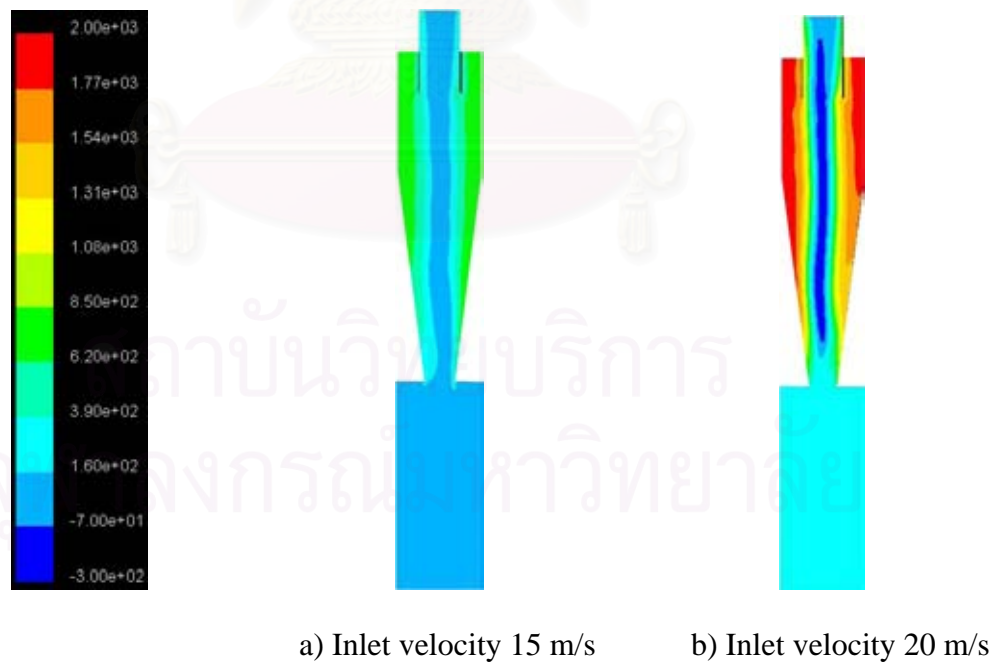
Figure 6.4.2 Measured collection efficiency by Dirgo and Leith (1985) and simulated results for cyclone type II

a) Inlet velocity 15 m/s   b) Inlet velocity 20 m/s

Figure 6.4.3 Contour of tangential velocity in cyclone type II

a) Inlet velocity 15 m/s   b) Inlet velocity 20 m/s

**Figure 6.4.4** Contour of pressure distribution in cyclone type II

6.4.2 Effect of blowdown ratio

To investigate the effect of blowdown ratio on collection efficiency and pressure drop of the cyclone type II is the objective of this section.

Figure 6.4.5 shows the effect of blowdown ratio on cyclone collection efficiency. It is clearly seen that the collection efficiency is better when the ratio of blowdown is increased. Especially, the sub-micron particle can be more collected from 3% to 15% when the ratio of blowdown is increased to 15%. In addition, the ratio of blowdown affects to the cut size that is decreased from 2.8 to 2 micron.

Table 6.4.1 lists the effect of increasing blowdown ratio on the pressure drop of cyclone type II. It should be noted that this pressure drop is obtained by calculating the difference of pressure between the inlet and outlet pipe of cyclone. In case of blowdown, the simulated pressure drop is slightly higher when the ratio of blowdown is increased from 0% to 15%.

In short, the better collection efficiency and cut size are provided by aspiring air at the upper part of hopper section of cyclone type II. This method can improve the cyclone performance to collect or separate the sub-micron particles from fluid stream as the pressure drop is slightly increased.
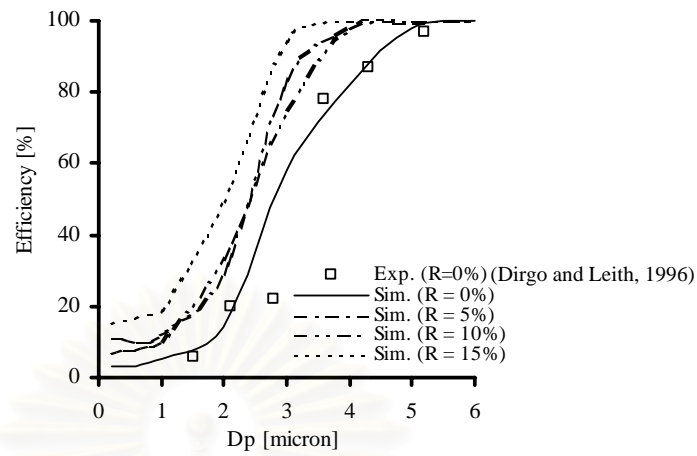
Figure 6.4.5 Effect of the ratio of blowdown on collection efficiency.

Inlet velocity = 15 m/s

Table 6.4.1 Effect of blowdown ratio on pressure drop across cyclone type II

Ratio of blowdown [%]	Pressure drop [Pa] Experimental[1]	Pressure drop [Pa] Simulation
0	785	701
5	-	736
10	-	764
15	-	826

[1] Experimental from Dirgo and Leith (1985)

There are two components of velocity are important for particle collection within cyclone. The axial velocity conducts particle to move into the dust hopper and tangential velocity affect to centrifugal force that act on particle to collide with wall.

Figure 6.4.6 illustrates the contour of axial velocity in cyclone type II. It can be seen that the downward velocity at the lower part of conical section has the higher magnitude when the ratio of blowdown is increased. Therefore, the opportunity of the particles traveling into the dust hopper is also higher. **Figure 6.4.7** illustrates that the tangential velocity in cylindrical and conical section increases as ratio of blowdown is increased.

Figure 6.4.8 illustrates that the withdrawn air affect to the pressure contour. In case with blowdown, it can be observed that pressure near the wall of cyclone becomes higher while the pressure in core region becomes lower. It can be imply that this system has higher energy loss near the both of cylindrical and conical wall.

a) R = 0%   b) R = 10%
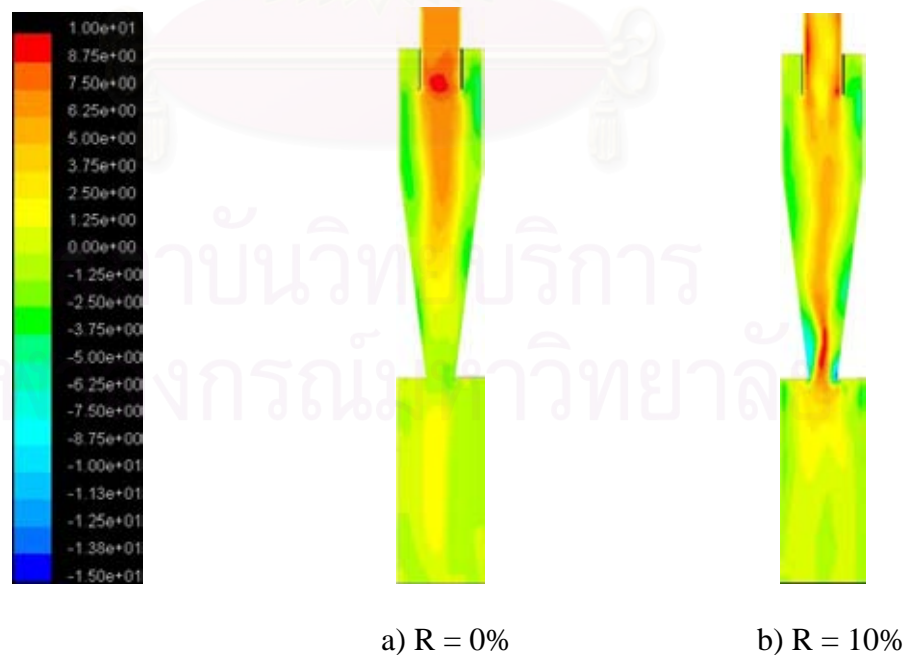
Figure 6.4.6 Effect of the ratio of blowdown on axial velocity in cyclone type II

a) R = 0%   b) R = 10%
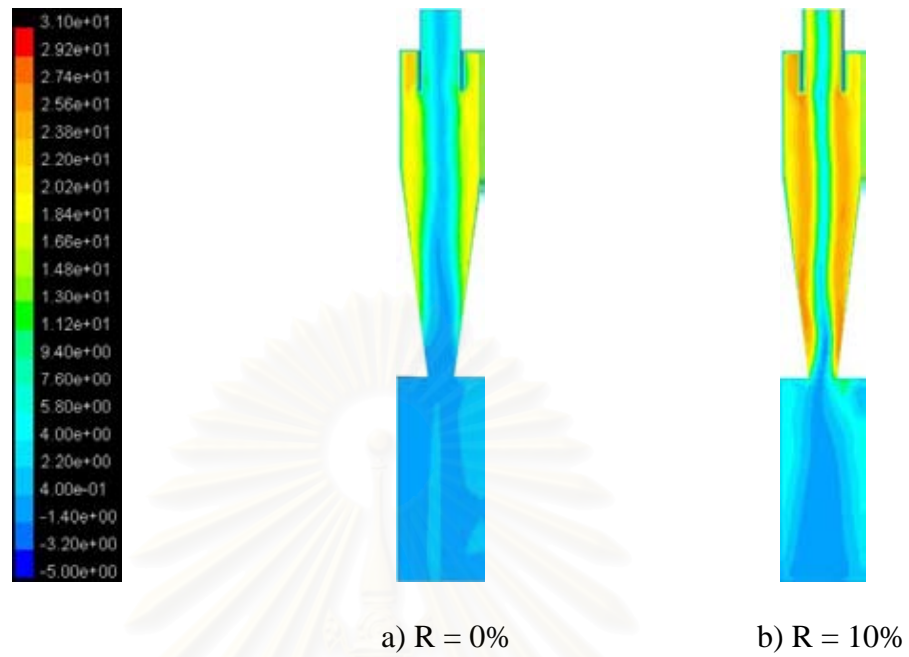
Figure 6.4.7 Effect of the ratio of blowdown on tangential velocity in cyclone type II

a) R = 0%   b) R = 10%
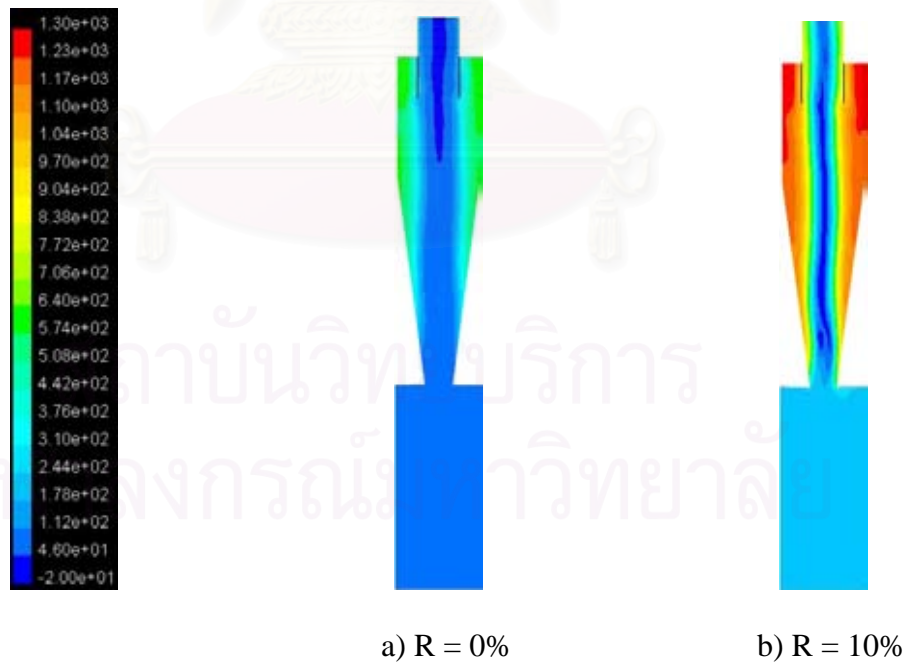
Figure 6.4.8 Effect of blowdown ratio on pressure in cyclone type II

6.4.3 Effect of 10% blowdown at various inlet air velocities

The comparison of pressure drop of cyclone with 10% blowdown at the various inlet air velocities is listed in **Table 6.4.2**. At first, it should be mention that our simulation results are greatly agreement with experimental from Dirgo and Leith (1985). The deviation of experimental data with simulation result is about 8-12%. In case of blowdown, it can be found that the pressure drop is increased about 13%, 9%, 16% and 17% as the inlet velocity of 10 m/s, 15 m/s, 20 m/s, 25 m/s with blowdown, respectively.

Figure 6.4.9 shows the effect of 10% blowdown at various inlet air velocities on collection efficiency. F**igure 6.4.9 a)** illustrates that the blowdown slightly affects to the collection efficiency especially the particle size is smaller than cut size. However, the collection efficiency for large particle becomes higher when the ratio of blowdown is increased due to higher centrifugal force.

Figure 6.4.9 b) - 6.4.9 c) show that the collection efficiency significantly increase as blowdown ratio increases to 10%. The blowdown affects to collect sub-micron particles. This particle size is more collected by aspiring air 10% by volume from upper part of hopper section.

In short, all range of particle size can be more collected when the inlet air velocity of cyclone type II is 10-20 m/s as ratio of blowdown is 10%.

Figure 6.4.9 d) shows that the 10% ratio of blowdown does not affect the collection efficiency of cyclone type II with inlet air velocity of 25 m/s. It can be mention that pressure at core region is decreased as inlet velocity increases. Therefore, the possibility of the sub-micron particle becomes higher.
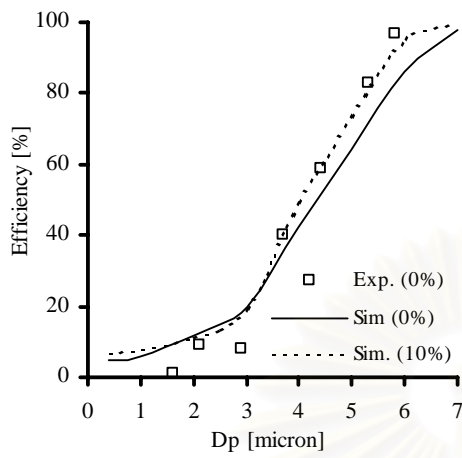
Table 6.4.2 Effect of 10% blowdown on pressure drop at various inlet air velocities

	Pressure drop [Pa]		
	Experimental[1]	Simulation	
	R = 0%	R = 0%	R = 10%
v = 10 m/s	337	310	352
v = 15 m/s	785	701	764
v = 20 m/s	1,407	1,237	1,438
v = 25 m/s	2,205	1,972	2,302

[1] Experimental results from Dirgo and Leith (1985)
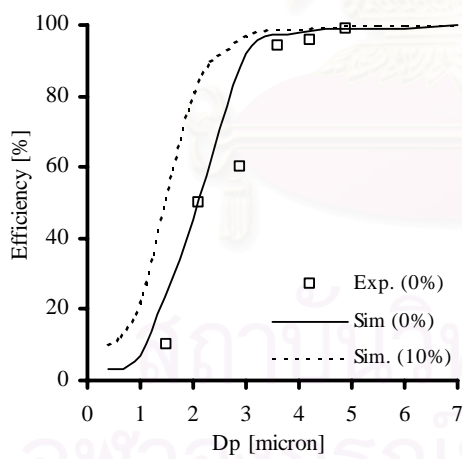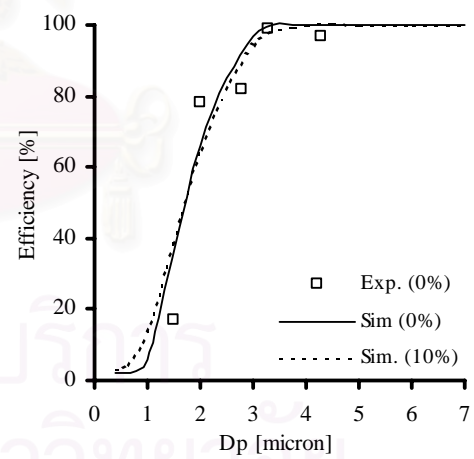
a) inlet air velocity 10 m/s
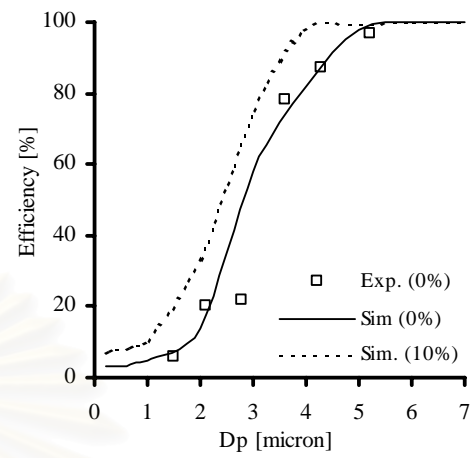
b) inlet air velocity 15 m/s

c) inlet air velocity 20 m/s

d) inlet air velocity 25 m/s

**Figure 6.4.9** Effect of 10% blowdown ratio on collection efficiency

6.4.4 Effect of particle inlet positions

The effect of particle inlet positions on the opportunity of particle collection in cyclone type II with inlet air velocity of 15 m/s can be investigated by injecting a particle into the across section area of inlet pipe. This inlet plane is divided into four regions as shown in **Figure 6.4.10**.

The simulated particle size is 1,3 and 5 micron for investigating the particle trajectory because these particle sizes are between the cut size ($D_{50} \approx 3$ micron). The detail of trajectory, a particle of 1 micron cannot reach to wall as shown in **Figure 6.1.11** while a particle of 3 micron ($D_{50} \approx 3$ micron) can be collected when it is injected into region III and IV as shown in **Figure 6.1.12**. Finally, a particle with 5 micron can be collected for all injected area as shown in **Figure 6.1.13**.

The results of simulation show that opportunity of a fine particle collection becomes higher when this particle is injected into region III or region IV because it can move into the free-vortex finder. The direction of axial velocity in this free-vortex finder is downward direction so a small particle is inducted to the hopper section to collect in cyclone. In other hand, a fine particle is injected into region I or II has lower opportunity of particle collection because this particle slips down on the wall of vortex finder and swirls up to escape from cyclone. However, the particle inlet position slightly affects to the opportunity of particle collection when particle size is larger than the cut size due to it has higher centrifugal force.

In short, the result of this simulation can be concluded that region IV is the highest effective region because the particle of all size can be collided to the wall of cyclone. The lower effective zone is region III, II and I, respectively.
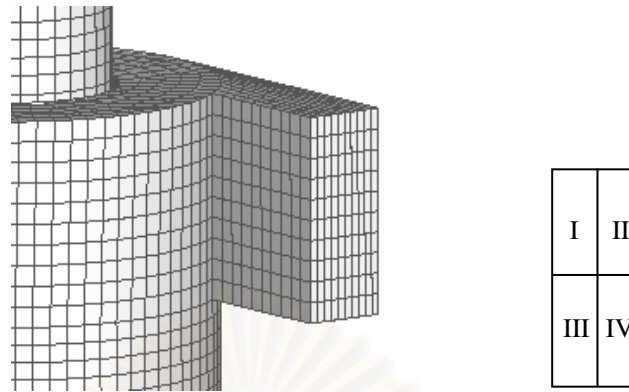
Figure 6.4.10 Four regions of inlet plane for cyclone type II
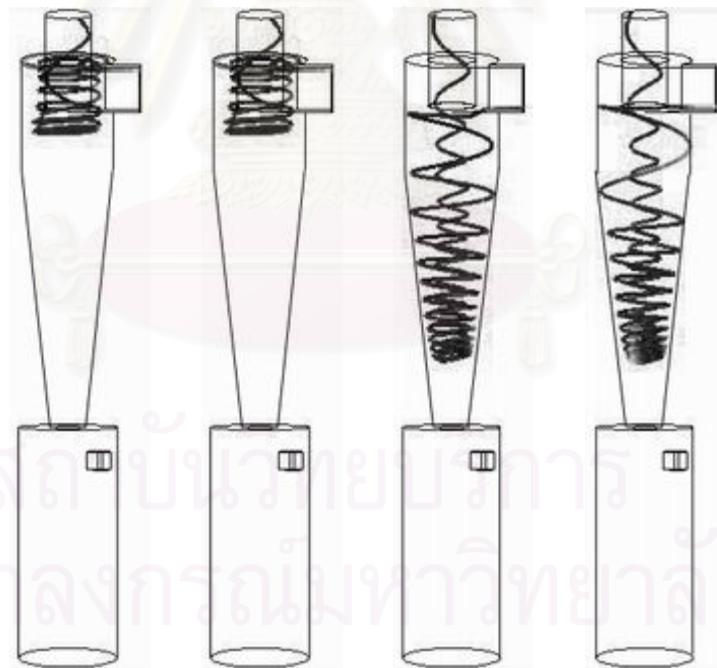
a) region I   b) region II   c) region III   d) region IV

Figure 6.4.11 Trajectory of particle with 1 micron in cyclone type II
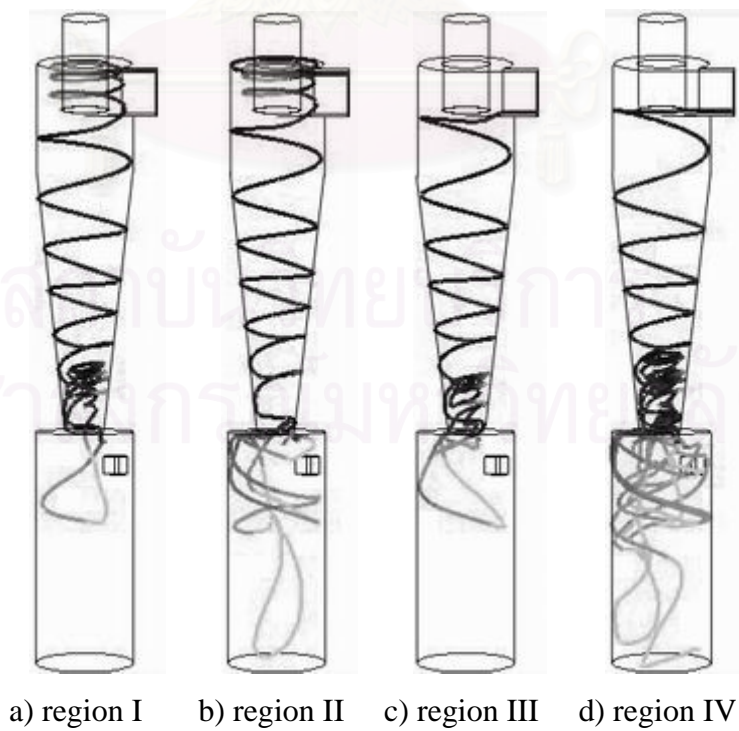
a) region I   b) region II   c) region III   d) region IV
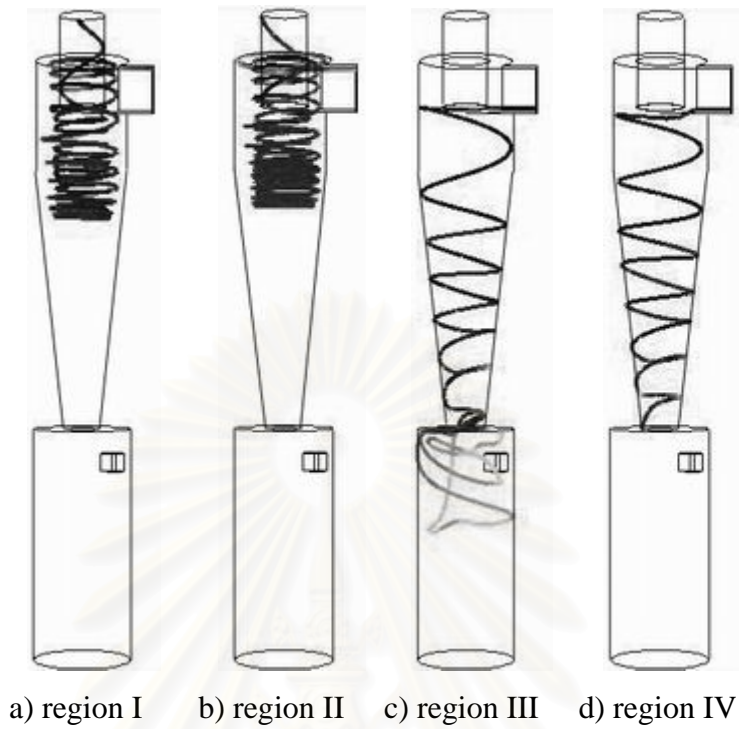
Figure 6.4.12 Trajectory of particle with 3 micron in cyclone type II

a) region I   b) region II   c) region III   d) region IV

Figure 6.4.13 Trajectory of particle with 5 micron in cyclone type II

CHAPTER VII

CONCLUSIONS AND RECOMMENDATIONS

7.1 Conclusions

The following conclusions are obtained by simulating the fluid dynamics and particle trajectory along 3-dimensional turbulent flow in air cyclones installed with blowdown pipe.

1. The Reynolds Stress Model (*RSM*) can provide prediction of fluid dynamics and particle trajectory in cyclones better those of the Standard $k - \varepsilon$ and $RNG - k - \varepsilon$ turbulent models due to its non-isotropic assumption.

2. As inlet air velocity increases, more amounts of sub-micron particles could be collected while pressure drop is also increased proportionally to the square of inlet air velocity.

3. The collection efficiency becomes higher when the ratio of blowdown is increased due to the increasing opportunity of particles to collect within dust hopper.

4. Withdrawing a small amount of air from hopper section provides the better collection efficiency and lower pressure drop. Effect of blowdown is more significant that of the increasing inlet velocity.

5. The most effective zone for particle collection is close to the outer wall at bottom of inlet pipe because the inlet particle can swirl down into semi-free vortex.

7.2 Recommendations

1. This research does not take into account the high concentration of inlet particle. This parameter could affect particle collection due to its particle - particle interaction, and it is necessary for determining cyclone performance.

2. To supply the electrical voltage at wall of cyclone may increase the cyclone collection efficiency especially for sub-micron particle. The transport phenomenon of fluid dynamics and particle trajectory in this system is difficultly obtained by experimental method. Therefore, numerical simulation will be possible mean to get such information.

REFERENCES

Abrahamson, J., Jones, R.,Lau, A. and Reveley, S.. Influence of entry duct bends on the performance of return-flow cyclone dust collectors. Powder technology 123 (2002) : 126–137.

Altmeyer, S., Mathieu, V., Jullemier, S., Contal, P., Midoux, N., Rode, S., Leclerc, J. P.. Comparison of different models of cyclone prediction performance for various operating conditions using a general software. Chemical engineering and processing 43 (2004) : 511-522.

Bay, M. B., Luning, P. E., Hoffmann, A. C.. Post cyclone (PoC): An inovative way to reduce the emission of fines from industrial cyclones. Ind. Eng. Chem. Res. 36 (1997) : 2766 - 2774.

Bird, R.B., Stewart, W.E. and Lightfoot, E.N. . Transport phenomena. New York : John Wiley, 2002.

Blazek, J.. Computational fluid dynamics: Principles and applications. Oxford : Elsevier science, 2001.

Ceylan, K., Herdem, S. and Abbasov, T.. A theoretical model for estimation of drag force in the flow of non-newtonian fluids around spherical solid particles. Powder technology 103 (1999) : 286-291.

Chung, T.J.. Computational fluid dynamics : Cambridge university press, 2002.

Clift, R., Ghadiri, M.. A critique of two models for cyclone performance. AIChe Journal 37 (February 1991) : 285-289.

Crowe, C., Sommerfeld, M., Tsuji Y.. Multiphase flows with droplets and particles. New York : CRC Press, 1998.

Dirgo, J., Leith, D.. Cyclone collection efficiency : comparison of experimental results with theoretical predictions. Aerosol science and technology 4 (1985) : 401-415.

Ferziger, J. H. and Peric, M.. Computational methods for fluid dynamics. 2 nd ed. Berlin : Springer-Verlag, 1999.

Fredriksson, C.. Exploratory experimental and therectical studies of cyclone gasification of wood powder. Lulea tekniska university (1999) : 1-145.

Gimbun, J., Chuah T.G., Razi, A., Choong, T.S.Y.. The influence of temperature and inlet velocity on cyclone pressure drop: a CFD study. Chemical engineering and processing 44 (2005) : 7-12.

Griffiths, W.D. and Boysan, F.. Computational fluid dynamics (CFD) and empirical modelling of the performance of a number of cyclone samplers. Aerosol Science 27 (March 1996) : 281-304.

Heiskanen, K.. Particle classification. London : Kluwer Academic Pub, 1993.

Hoekstra, A. J., Derksen, J.J., Van Den Akke, H.E.A. . An experimental and numerical study of turbulent swirling flow in gas cyclones. Chemical engineering science 54 (July 1999) : 2055-2065.

Huber, N. and Sommerfeld, M. . Modelling and numerical calculation of dilute-phase pneumatic conveying in pipe system. Powder technology 99 (September 1998) : 90-101.

Iinoya, K., Gotoh, K., Higashitani, K.. Powder technology handbook. 1 st ed. New York : Marcel dekker, 1990.

Kim, J. C., Lee, K. W.. Experimental study of particle collection by small cyclones. Aerosol science and technology 12 (1990) : 1003-1015.

Ma, L., Ingham, D. B., Wen, X.. Numerical modeling of the fluid and particle penetration through small sampling cyclones. Aerosol science 31 (2000) : 1092-1119.

Obermair, S., Woisetschlager, J., Staudinger, G.. Investigation of the flow pattern in different dust outlet geometries of a gas cyclone by laser doppler anemometry. Powder technology 138 (December 2003) : 239-251.

Okawa, A. Mechanical separation process and flow pattern of cyclone dust collectors, 1997.

Parker, C.. Aerosol science and technology. New York : McGraw-Hill, 1993.

Patankar, S.V. . Numerical heat transfer and fluid flow. London : Hemisphere, 1980.

Patankar, S.V. and Spalding, D.B.. Calculation procedure for heat, mass and momentum transfer in three-dimensional parabolic flows. International journal heat mass transfer 15 (October 1971) : 1787-1806.

Patterson, P.A. and Munz, R. J.. Gas and particle flow pattern in cyclone at room elevated temperature. Chemical engineer 74 (1996) : 213-221.

Peng, W., Boot, P. J. A. J. and Hoffmann, A. C.. Flow in the inlet region in tangential inlet cyclones. Ind. Eng. Chem. Res. 40 (2001) : 5649-5655.

Tannehill, J.C., Anderson, D.A., and Pletcher, R.H.. Computational fluid mechanics and heat transfer. 2 nd ed. Philadelpia : Taylor&Francis, 1997.

Versteeg, H. K. and Malalasekera, W.. An introduction to computational fluid dynamics : The finite volume method: Addison wesley longman, 1995.

William, C.H.. Aerosol technology. 2 nd ed. Canada : John Wiley, 1999.

Wirz, H.J., Smolderen, J.J.. Numerical methods in fluid dynamics. London : Hemisphere, 1978.

Xiaodong, L., Jianhua, Y., Yuchun, C., Mingjiang, N., Kefa C.. Numerical simulation of the effects of turbulence intensity and boundary layer on separation efficiency in a cyclone separator. Chemical engineering journal 95 (2003) : 235-240.

Yang, K. S., Yoshida, H.. Effect of mist injection position on particle separation performance of cyclone scrubber. Separation and purification technology 37 (2004) : 221-230.

Yoshida, H., Fukui, K., Yoshida, K., Shinoda, E.. Particle separation by Iinoya's type gas cyclone. Powder technology 118 (2001) : 16-23.

Yoshida, H.. Three-dimensional simulation of air cyclone and particle separation by a revised-type cyclone. Colloids and surfaces 109 (April 1996) : 1-12.

Zhao, B., Shen, H., Kang, Y.. Development of a symmetrical spiral inlet to improve cyclone separator performance. Powder technology 145 (2004) : 47-50.

APPENDICES
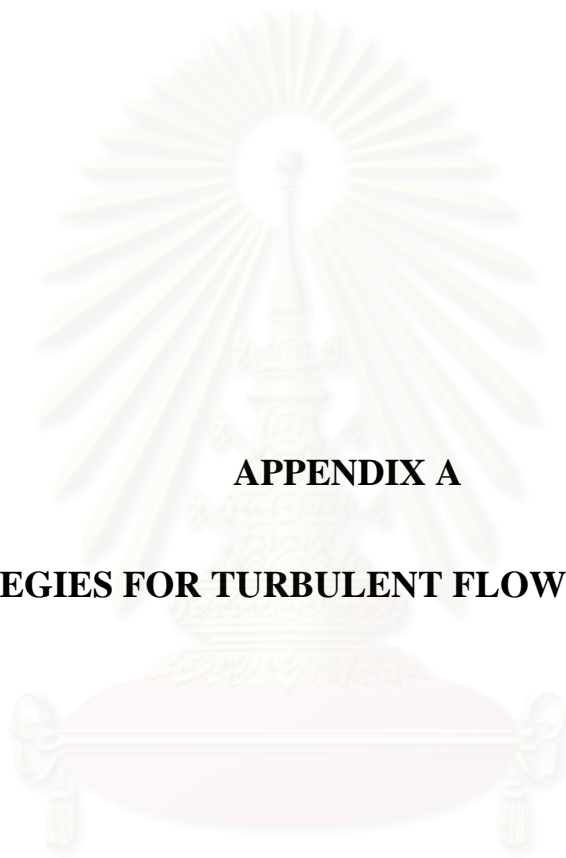
APPENDIX A

STRATEGIES FOR TURBULENT FLOW SIMULATION

Strategies for Turbulent Flow Simulations

Compared to laminar flows, simulations of turbulent flows are more challenging in many ways. For the Reynolds-averaged approach, additional equations are solved for the turbulence quantities. Since the equations for mean quantities and the turbulent quantities (μ_t, k, ε or R_{ij}) are strongly coupled in a highly non-linear coupling, it takes more computational effort to obtain a converged turbulent solution than to obtain a converged laminar solution. These suggestions will help to obtain better accuracy results.

Mesh Generation: Too fine or too coarse is avoided to generate. In case of too fine mesh, the consumption of computational effort and memory is very high. In opposite, the low accuracy will occur when too coarse is employed. The appropriate grid size can be obtained by optimizing between computational time and accuracy of solution.

Accuracy: The recommendation for the convection terms is that high-order schemes should be employed. The QUICK is the recommended scheme for interpolating the convection term. Especially, this scheme should be employed when flow is high Reynolds number and high rotational flow as well as fluid dynamics in cyclone separator.

Convergence: Starting with excessively initial guesses for mean and turbulence quantities may cause the solution to diverge. A safe approach is to start your calculation using small under-relaxation parameters, and increase them gradually as the iterations proceed and the solution begins to settle down.

When $RNG-k-\varepsilon$ model is employed, to use standard $k-\varepsilon$ turbulent model can help to achieve better convergence before switching to the $RNG-k-\varepsilon$ model. In short, the solution of lower accuracy turbulent model is the initial value of higher accuracy turbulent model.

RSM-Specific Solution Strategies

A high degree of coupling between the momentum equations and the turbulent stresses in the flow is occur when *RSM* turbulent model is employed, and thus the calculation is more difficult for stability and convergence than the standard $k - \varepsilon$ or $RNG - k - \varepsilon$ turbulent models. The following strategies are generally recommended.

Under-Relaxation of the Reynolds Stresses: The default under-relaxation is 0.5 for the most cases. In general, the rate of convergence will be increase if this under-relaxation is also increased. However, the 0.2-0.3 under-relaxation factor is our recommendation for highly swirling flows or highly complex flows as well as fluid flow field in cyclone. For Reynolds Stress Model, the under-relaxation factors both for the velocities and for all of the Reynolds stress components should be set to 0.2 - 0.3. In our simulated experience, the divergence solution can be occurred when the setting of under-relaxation is 0.6 or larger.

Residual error for the RSM: When the eddy-viscosity model as Standard $k - \varepsilon$ (SKE) or $RNG - k - \varepsilon$ turbulent models are employed, the range of residual error can be set to 10^{-3}. However, this residual error for Reynolds Stress Model should be set lower than 10^{-6}.

The quality of mesh generation: The effect of resolution, smoothness and cell shape on the accuracy and stability of the solution process is strongly dependent on the flow field. For example, much skewed cells can be very damaging in regions with strong flow gradients. Therefore, a high-quality mesh over the entire flow domain should be aware.

APPENDIX B

INTRODUCTION TO FLUENT 6.1.22 AND GAMBIT 2.1.6

Introduction to FLUENT 6.1.22 and GAMBIT 2.1.6

FLUENT is a commercial program for modeling fluid flow and heat transfer in complex geometries. This program provides complete mesh flexibility, solving the flow problems with unstructured meshes that can be generated about complex geometries. The supported mesh types include 2D with triangular/quadrilateral or 3D with tetrahedral/hexahedral/pyramid/wedge, and mixed (hybrid) meshes.

FLUENT is written in the C computer language and makes full use of the flexibility and power offered by the language. Consequently, true dynamic memory allocation, efficient data structures, and flexible solver control are all made possible.

The GAMBIT software package is designed to help analysts and designers build and mesh models for computational fluid dynamics (CFD) and other scientific applications. Additional, TGrid can also generate a triangular, tetrahedral, or hybrid volumes mesh. It is also possible to create grids for FLUENT using ANSYS or NASTRAN Interfaces to other CAD/CAE packages. Once a grid has been read into FLUENT, all remaining operations are performed within this solver program. These include setting boundary conditions, defining fluid properties, executing the solution, refining the grid, and viewing and post processing the results.

This commercial code package includes the following products

- FLUENT is the solver, as shown in **figure B.1**.
- PrePDF is the preprocessor for modeling non-premixed combustion.
- GAMBIT is the preprocessor for mesh generation as shown in **figure B.2**.
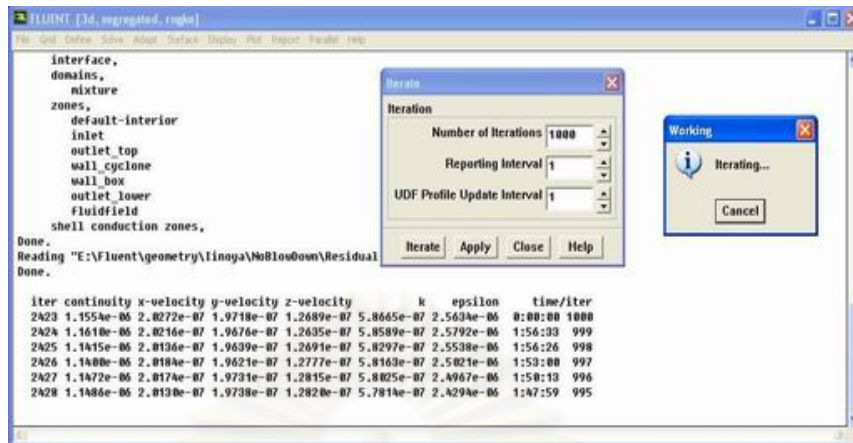- Tgrid is an additional preprocessor that can generate volume meshes

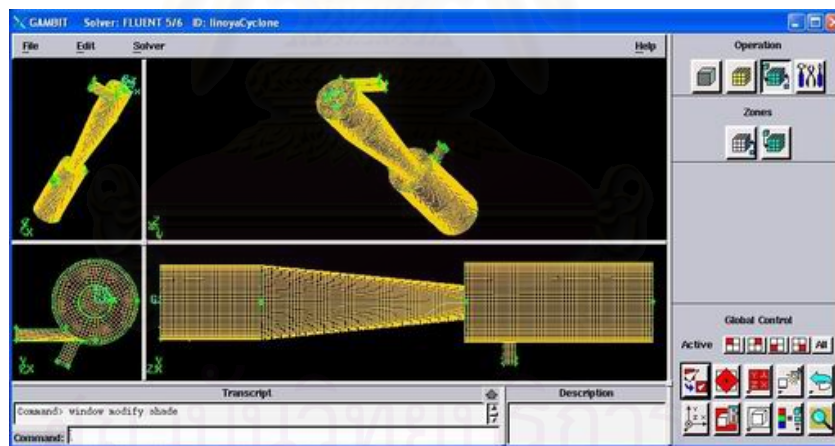**Figure B.1** Preface of the FLUENT release 6.1.22

Figure B.2 Preface of the GAMBIT release 2.1.6

VITA

Mr. Kompanart Kaewplang was born on June 16, 1978 in Bangkok, Thailand, the second son of Mr. Roumsak and Mrs. Somtawil Kaewplang. He attended Bodindecha2 School in Bangkok and graduated in 1996. In March 2000, he received his Bachelor Degree of Engineering in Chemical Engineering from faculty of Engineering, Thammasat University. After graduation, he had worked for Thai Petrochemical Industry Co., Ltd (Public) on an engineer in position of Logistic Planning (LP) section. He got admission to the Graduate School of Chulalongkorn University and is awarded the degree of Master of Engineering in Chemical Engineering in academic year 2004.